PCCP

PERSPECTIVE

View Article Online
View Journal | View Issue

Cite this: *Phys. Chem. Chem. Phys.*, 2016, **18**, 11589

Beyond organic chemistry: aromaticity in atomic clusters

Alexander I. Boldyrev*[a] and Lai-Sheng Wang*[b]

We describe joint experimental and theoretical studies carried out collaboratively in the authors' labs for understanding the structures and chemical bonding of novel atomic clusters, which exhibit aromaticity. The concept of aromaticity was first discovered to be useful in understanding the square-planar unit of Al_4 in a series of MAl_4^- bimetallic clusters that led to discoveries of aromaticity in many metal cluster systems, including transition metals and similar cluster motifs in solid compounds. The concept of aromaticity has been found to be particularly powerful in understanding the stability and bonding in planar boron clusters, many of which have been shown to be analogous to polycyclic aromatic hydrocarbons in their π bonding. Stimulated by the multiple aromaticity in planar boron clusters, a design principle has been proposed for stable metal-cerntered aromatic molecular wheels of the general formula, $M@B_n^{k-}$. A series of such borometallic aromatic wheel complexes have been produced in supersonic cluster beams and characterized experimentally and theoretically, including $Ta@B_{10}^-$ and $Nb@B_{10}^-$, which exhibit the highest coordination number in two dimensions.

Received 3rd December 2015,
Accepted 28th January 2016

DOI: 10.1039/c5cp07465g

www.rsc.org/pccp

Published on 28 January 2016. Downloaded by Brown University on 04/02/2017 04:05:37.

1. Introduction

The year 2015 marks the 150th anniversary of the introduction of the concept of aromaticity in chemistry. In 1865, Kekule published his landmark papers,[1–3] where he first used the term aromaticity to explain the particular stability and low reactivity of a class of molecules related to benzene and its derivatives. In 1931, Hückel formulated his famous $4n + 2$ rule.[4,5] It states that if an unsaturated cyclic hydrocarbon molecule has the right number of π-electrons obeying this rule, then the molecule is aromatic and has high stability and low reactivity. In 1970, Breslow introduced the concept of antiaromaticity,[6,7] which implies the destabilization of cyclic unsaturated hydrocarbons with $4n$ π-electrons. Antiaromatic molecules are more reactive than non-aromatic molecules. The concept of aromaticity was confined primarily to the realm of organic chemistry. However, with the quantum mechanical understanding of the underlying causes of aromaticity and advances in experimental techniques to create novel molecules and clusters, the concepts of aromaticity and antiaromaticity have found wider applicability far beyond organic chemistry.[8–18] There is a huge amount of literature and rich history for aromaticity beyond organic chemistry since Kekule. A comprehensive review of the development of the concepts of aromaticity and antiaromaticity over the last 150 years is beyond the scope of this Perspective. Instead, this article traces a more or less personal journey of the authors in their collaborative endeavors in recent years.

Since about the end of the 1990s, the Boldyrev and Wang groups have initiated major experimental and theoretical collaborations to elucidate the structures and chemical bonding of many nonstoichiometric molecular and size-selected cluster systems.[19–21] This Perspective will start from the discovery of all-metal aromaticity in 2001[22] and how to use the concepts of aromaticity and antiaromaticity to understand the structures and bonding in metal and non-metal cluster systems. A previous Perspective and a comprehensive review article have been devoted to the metallic systems.[8,23] In the current Perspective, we will recap the idea of aromaticity in metal clusters and will mainly focus on planar boron clusters, for which not only the aromaticity concept emerges naturally, but it is also essential for the understanding of the planarity and stability of the planar boron clusters. In particular, the π bonding in planar boron clusters has been found to be directly analogous to that in polycyclic aromatic hydrocarbons (PAHs). Even more exciting, using the knowledge about the bonding and aromaticity in planar boron clusters, we have proposed a design principle for transition metal centered boron molecular wheels ($M@B_n^-$). Several classes of such aromatic borometallic clusters have been produced and characterized, some of which may be subjected to large-scale laboratory syntheses if appropriate ligands and conditions can be found.

---

[a] *Department of Chemistry and Biochemistry, Utah State University, Logan, Utah 84322, USA. E-mail: a.i.bodyrev@usu.edu*

[b] *Department of Chemistry, Brown University, Providence, Rhode Island, 02912, USA. E-mail: lai-sheng_wang@brown.edu*

This journal is © the Owner Societies 2016

Published on 28 January 2016. Downloaded by Brown University on 04/02/2017 04:05:37.

2. Aromaticity in metal clusters

2.1. Al_4^{2-}: the first all-metal aromatic cluster

At the turn of this millennium, we observed and characterized several pentaatomic planar carbon molecules, in which Al and Si were used as the ligands around a central carbon atom.[24–26] We were interested in finding relationships between the geometric structures of these anti-van't Hoff molecular systems and their chemical bonding. This endeavour led us to examine other bimetallic aluminium clusters, such as $LiAl_4^-$, $NaAl_4^-$, and $CuAl_4^-$.[22] The Wang lab successfully produced these clusters using a laser vaporization supersonic cluster source and obtained well-resolved photoelectron spectra. Computational searches of the global minimum structures for these three anionic bimetallic clusters (MAl_4^-) by the Boldyrev group found that the most stable structures were square-pyramidal with the M atom sitting on a perfect Al_4 square cluster (Fig. 1a).

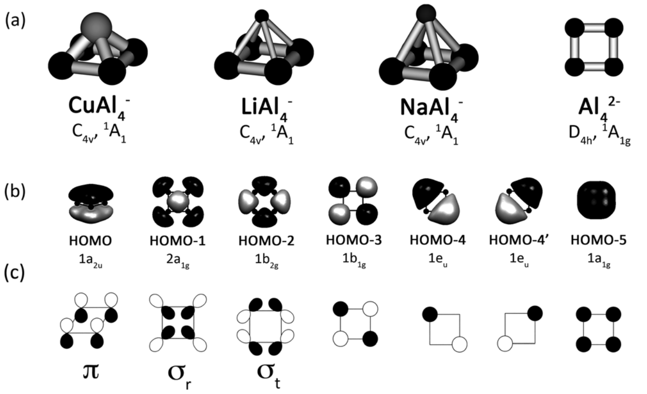

Fig. 1 (a) The global minimum structures of the MAl_4^- clusters (M = Cu, Li, Na) and the isolated Al_4^{2-} cluster; (b) the valence canonical molecular orbitals (CMOs) of the isolated Al_4^{2-} cluster; (c) schematic representation of the valence CMOs as linear combinations of the $3p_z$ atomic orbitals (AOs) comprising the highest occupied molecular orbital (HOMO, π), the 3p-radial AOs (HOMO−1, σ_r), the 3p-tangential (HOMO−2, σ_t), as well as the four different linear combinations of the 3s AOs (HOMO−3, HOMO−4, HOMO−4′, and HOMO−5).

The computed vertical electron detachment energies (VDEs) for these pyramidal structures were found to be in an excellent agreement with the experimental photoelectron spectra, confirming the identified pyramidal global minimum structures. In order to understand why these bimetallic clusters adopt these pyramidal structures, we further investigated the structure and bonding of the isolated Al_4^{2-} dianion, which was similar in all the bimetallic clusters. Even though the isolated Al_4^{2-} dianionic

Alexander I. Boldyrev

Alexander I. Boldyrev was born in Siberia, Russia (1951), and received his BS/MS (1974) in chemistry from Novosibirsk University, his PhD in physical chemistry from Moscow State University (1978), and his Dr Sci. in chemical physics from Moscow Physico-Chemical Institute (1987). He is currently a professor in Department of Chemistry and Biochemistry at Utah State University. His current scientific interest is the development of chemical bonding models capable of predicting the structure, stability, reactivity, and other molecular properties of molecules, pure and mixed clusters, low-dimensional materials and solids.

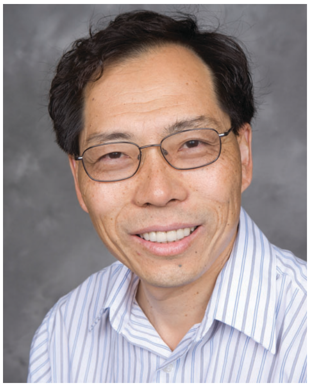

Lai-Sheng Wang

Lai-Sheng Wang received his bachelor degree in Chemistry from Wuhan University and his PhD from the University of California at Berkeley. After a postdoctoral stay at Rice University, he took a joint position between Washington State University and Pacific Northwest National Laboratory in 1993, and then moved to Brown University as Professor of Chemistry in 2009. He is currently the Jesse H. and Louisa D. Sharpe Metcalf Professor of Chemistry at Brown University. One major research topic in the Wang Lab focuses on the investigation of the fundamental behaviors of nanoclusters using photoelectron spectroscopy. Research in his group has led to the discovery of the golden buckyballs and golden pyramids, as well as aromatic clusters and planar boron clusters. He and his collaborators discovered borospherenes (boron cage clusters) and the first experimental evidence for the viability of borophenes (atomically thin boron monolayers). His group has also pioneered spectroscopy studies in the gas-phase of free multiply charged anions and complex solution-phase anions, such as metal complexes, redox species, and biologically relevant molecules. His group developed the cryogenically cooled quadruple ion trap to create ultracold singly and multiply charged anions from an electrospray source for high-resolution photoelectron spectroscopy. His group has also been developing resonant photoelectron spectroscopy via dipole-bound excited states of cryogenically cooled anions.

This journal is © the Owner Societies 2016

Published on 28 January 2016. Downloaded by Brown University on 04/02/2017 04:05:37.

cluster was not electronically stable by itself, it could be optimized using compact basis sets and its electronic and geometric structures were found to be similar to those in the pyramidal MAl_4^- clusters (Fig. 1a). Further details on this topic can be found in ref. 27 and 28. An obvious question was why the Al_4^{2-} dianion had a square-planar structure, instead of the expected tetrahedral structure. It should be mentioned that at that time the prevailing electronic model for metal clusters was the jellium model,[29,30] which assumed a metal cluster as a structureless ionic jelly permeated by itinerant electrons. A more compact tetrahedral structure would have been anticipated for Al_4^{2-} from the jellium model.

Analyses of the chemical bonding using the CMOs shown in Fig. 1b and c revealed that HOMO−5 to HOMO−3 corresponded to four lone pairs ($3s^2$), one on each Al atom. The remaining three CMOs (HOMO to HOMO−2) were responsible for the chemical bonding in Al_4^{2-}. The HOMO was a π-bonding CMO, giving rise to π-aromaticity according to the Huckel rule. HOMO−1 and HOMO−2 were delocalized σ-bonding CMOs. HOMO−1 was responsible for the radial overlap of the 3p-AOs and HOMO−2 was responsible for the tangential overlap of the 3p-AOs (Fig. 1c), giving rise to σ-aromaticity. In the original article only π-aromaticity was emphasized,[22] out of an abundance of caution, fearing that invoking σ-aromaticity might be too controversial. Interestingly, Fowler and co-workers immediately showed that the Al_4^{2-} dianion was more σ-aromatic than π-aromatic![31,32] However, Sola and co-workers[33] reported that according to the electronic multicenter indices (MCIs) aromaticity gives similar weights to the σ and π aromaticities in Al_4^{2-}. Poater *et al.*[34] pointed out that the σ system and not the π one is responsible for the D_{4h} structure in Al_4^{2-}.

2.2. Aromatic Ga_4^{2-} and In_4^{2-}

Subsequently we reported joint photoelectron spectroscopy and theoretical results for the $NaGa_4^-$ and $NaIn_4^-$ clusters and showed that these heavier congeners of Al_4^{2-} had similar structures and bonding and all three species were doubly σ- and π-aromatic.[35] The electronic structure and chemical bonding in all these clusters could not be explained on the basis of the classical Lewis structure. It was also difficult to represent the chemical bonding using the Kekule-like resonance structures.[36,37] Havenith and van Lenthe[38] performed *ab initio* valence bond (VB) calculations, which incorporated natural resonance structures. Surprisingly, they found that the Dewar-like resonance structures with a diagonal bond had the highest weight. Many publications have subsequently examined the aromaticity of the Al_4^{2-} species in bimetallic MAl_4^- clusters and generally confirmed the presence of σ- and π-aromaticity. In some cases, these systems were suggested to be just σ-aromatic. More detailed discussions of these studies can be found in the 2005 review.[8]

It should be mentioned that in 1995 Robinson and co-workers reported π-aromaticity in the $[Na_2(Mes_2C_6H_3)Ga]_3$ (Mes = 2,4,6-$Me_3C_6H_2$) compound,[39] which contained a triangular aromatic Ga_3^{2-} ring embedded in a large organometallic molecule. More interestingly, Power and co-workers reported the synthesis and crystal structure of $K_2[Ga_4(C_6H_3\text{-}2,6\text{-}Trip_2)_2]$ (Trip = C_6H_2-2,4,6-iPr_3), which contained a square-planar Ga_4^{2-} unit in the center flancked by two K^+ ions.[40] We showed that the bonding in the ligand-protected Ga_4^{2-} was similar to that in our $NaGa_4^-$ cluster and correctly explained the bonding in this compound.[35] In fact, the Power compound could be viewed as the first synthetic realization of the all-metal aromatic M_4^{2-} (M = Al, Ga, In) clusters.

It was further demonstrated that aromaticity in heteroatomic metal clusters was also possible: the heterometallic MAl_3^- (M = Ge, Sn, Pb) clusters were all shown to possess similar aromaticity to the M_4^{2-} cluster.[41] Khanna and co-workers have also reported aromaticity in several heteroatomic metal clusters.[42–44]

2.3. Al_4^{4-}: an all-metal antiaromatic cluster

To further prove the validity of all-metal aromaticity would be to show all-metal antiaromaticity. The Wang and Bodyrev labs in fact searched quite extensively for such a system both experimentally and theoretically. It turned out that a simple solution was to add two more π electrons in Al_4^{2-} to create a 4 π-electron Al_4^{4-}, which should be rectangular, similar to the prototypical antiaromatic organic molecule, cyclobutadiene (C_4H_4). However, this quadruply charged anion was expected to be an extremely unstable species electronically and would need to be stabilized by counter ions, which was accomplished in 2003 in the form of $Li_3Al_4^-$.[45] The Wang lab successfully created this bimetallic cluster in a supersonic cluster beam using a Li–Al composite laser-vaporization target and measured its photoelectron spectrum. If charge transfers occurred from the Li atoms to the Al unit, this cluster should consist of an Al_4^{4-} unit coordinated and stabilized by three Li^+ ions. Computational searches for the global minimum structure of $Li_3Al_4^-$ by the Boldyrev group revealed many low-lying isomers (Fig. 2). The global minimum of this cluster indeed contained a rectangular Al_4^{4-} unit, slightly distorted by the asymmetric coordination of Li^+ (Fig. 2B). In fact, the neutral Al_4Li_4 cluster contained a perfectly rectangular Al_4^{4-} (Fig. 2A). Excellent agreement was found between the theoretical VDEs for the global minimum (C_s, $^1A'$) and the photoelectron data, confirming unequivocally the rectangular Al_4^{4-} unit in $Li_3Al_4^-$.

Chemical bonding analyses were performed to assess if the rectangular Al_4^{4-} unit in the bimetallic cluster was caused by antiaromaticity. The bonding CMOs for the $Li_3Al_4^-$ and Li_4Al_4 clusters are presented in Fig. 3, in comparison with those of Al_4^{2-} (Fig. 3A) and they were found to be very similar. Clearly, the Li atoms substantially donate electron densities to the Al_4 unit and the two clusters can be viewed approximately as $Li_3^+[Al_4^{4-}]$ and $Li_4^+[Al_4^{4-}]$. Compared to the MOs of Al_4^{2-} (Fig. 3A), the completely delocalized π MO (HOMO−4) is considerably stabilized in Al_4^{4-}. The two delocalized σ MOs (HOMO−1 and HOMO−2) correspond to the same set in Al_4^{2-} (Fig. 3A). The extra pair of electrons enters the HOMO of Al_4^{4-}, which is indeed a π-MO. This π-HOMO of Al_4^{4-} is bonding within the two shorter Al–Al bonds, but antibonding between the two pairs of Al (Fig. 3B), resulting in the rectangular shape and responsible for the antiaromatic character of Al_4^{4-}. Both the π-bonding pattern and the rectangular shape of Al_4^{4-} are indeed analogous to the prototypical antiaromatic cyclobutadiene.

View Article Online

Published on 28 January 2016. Downloaded by Brown University on 04/02/2017 04:05:37.

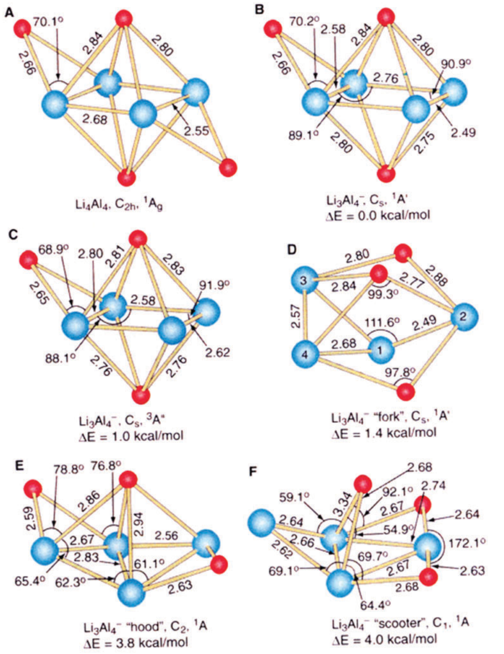

Fig. 2 Optimized structures of Li_4Al_4 and $Li_3Al_4^-$. Structural parameters given in Å and degrees are at the B3LYP/6-311+G* level of theory. The relative energies for the isomers of $Li_3Al_4^-$ are at the CCSD(T)/6-311+G(2df) level of theory.[45]

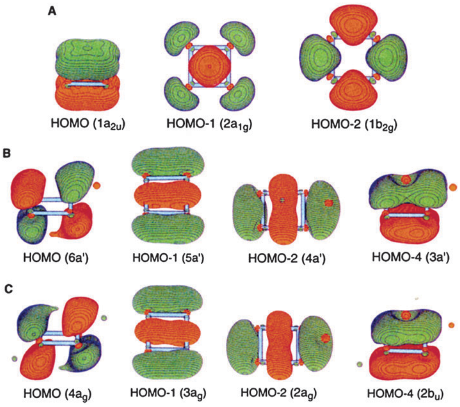

Fig. 3 Molecular orbital pictures for (A) Al_4^{2-} (D_{4h}, $^1A_{1g}$); (B) capped octahedral singlet $Li_3Al_4^-$ (C_s, $^1A'$); (C) Li_4Al_4 (C_{2h}, ^1A_g).[29]

Thus, Al_4^{4-} was the first all-metal π-antiaromatic species to be observed,[45] even though it still possessed σ-aromaticity derived from the two delocalized σ-bonding MOs.

However, Schleyer and co-workers disputed the antiaromaticity in $Li_3Al_4^-$.[46] They confirmed the global minimum structures for $Li_3Al_4^-$ and Li_4Al_4 shown in Fig. 2 and further computed the NICS indices for several isomers of $Li_3Al_4^-$, as well as for Li_4Al_4. They also confirmed that both the $Li_3Al_4^-$ and Li_4Al_4 ground states contained the rectangular Al_4^{4-} tetraanion motif with 4 π-electrons, which gave positive (paramagnetic) contributions to the NICS indices, *i.e.*, strongly π-antiaromatic. However, they obtained negative NICS indices for the σ electrons, confirming the σ-aromaticity in these bimetallic clusters, similar to that in Al_4^{2-}. When they added all the NICS indices from the π and σ electrons, they obtained an overall negative value because the magnitude of the NICS index from the σ electrons was higher than that from the π electrons. The total NICS values they obtained were: NICS($Li_3Al_4^-$) = −4.8 ppm and NICS(Li_4Al_4) = −11.4 ppm, from which they concluded that both systems should be considered net aromatic rather than net antiaromatic. Electronic indices of aromaticity support Al_4^{4-} as a σ aromatic and π antiaromatic species.[47]

There was an online discussion about the net aromaticity or antiaromaticity featured in *Chem. Eng. News*.[48] However, no consensus was reached. Many joined the discussion,[49–55] but there was still no consensus on this matter. See more detailed discussion of this issue in the 2005 review.[8] We still maintain that the $Li_3Al_4^-$ cluster is π-antiaromatic in the classical sense of the cyclobutadiene molecule, regardless of the aromaticity in the σ framework. In fact, the whole procedure to add the NICS values from the π and σ frameworks was questionable. They should be considered separately, *i.e.*, Al_4^{4-} is π antiaromatic and σ aromatic.

2.4. AdNDP: a new paradigm for chemical bonding analyses

It was clear from our early studies of the structures and bonding of novel clusters that we needed a new theoretical method for assessing aromaticity, which should not only allow us to localize all CMOs into lone pairs and two-center two-electron bonds, but also to find multi-center bonds. The Natural Bond Orbital (NBO) analysis developed by Weinhold and co-workers was an excellent tool to obtain the Lewis structure for a molecule if all bonding was restricted to lone pairs and two-center two-electron bonds.[56–59] However, in many cases we found that we needed to allow bonds to be delocalized over many atoms or all atoms if needed. The Boldyrev group decided to extend the NBO method to allow multi-center delocalized bonds. Zubarev from the Boldyrev group wrote the computer program and developed this method, which was called Adaptive Natural Density Partitioning (AdNDP).[60] In AdNDP, the search is first performed for localized lone pairs (1c-2e) and 2-center-2-electron (2c-2e) bonding elements. After the electron density responsible for localized bonding is removed, the search for the delocalized multi-center bonding elements or *n*c-2e bonds (*n* ranging from 3 to the total number of atoms in the system) is proceeded. The bonding elements recovered by AdNDP always correspond to the point group symmetry of the system, after these bonding elements are superimposed onto the molecular frame. The AdNDP method has been used in a wide variety of systems, including boron clusters to be discussed later in this article, prototypical aromatic hydrocarbons, gold clusters, organometallic complexes, and inorganic cluster complexes.[11,12,14–17,60] With AdNDP, aromaticity in organic and inorganic planar molecules can be assessed alternatively on the basis of the presence of delocalized chemical bonding. A chemical species is considered to be globally aromatic if there is a globally delocalized bonding element. Both the NBO and AdNDP methods were recently extended to periodic systems,[61,62] making it possible to analyze delocalized chemical bonding in 1D, 2D, and 3D systems.

Published on 28 January 2016. Downloaded by Brown University on 04/02/2017 04:05:37.

2.5. Hg_4^{6-}: all-metal aromaticity in amalgams and other solid compounds

Our all-metal aromatic Al_4^{2-} cluster reminded Prof. John Corbett about the amalgam Na_3Hg_2, which contained Hg_4^{6-} planar square units.[63] The Hg_4^{6-} unit was valence-isoelectronic to Al_4^{2-}, if the occupied d-AOs of Hg were ignored. Corbett first analyzed the structures and MOs for the Hg_4^{6-} unit in 1969.[64] We compared the CMOs of Hg_4^{6-} and Al_4^{2-} and found that they were indeed very similar.[65] Thus, the Na_3Hg_2 amalgam should be considered as a solid compound containing all-metal aromatic Hg_4^{6-} building blocks.

We further analyzed the bonding in Hg_4^{6-} using AdNDP, as shown in Fig. 4a. The advantage of the AdNDP results was that we could compare the bonding of the isolated Hg_4^{6-} unit with that embedded in the Na_3Hg_2 lattice (Fig. 4b).[14] For the isolated Hg_4^{6-} unit, the AdNDP analysis revealed four lone pairs (one for each Hg atom) and three completely delocalized bonds. The delocalized 4c-2e bonds were actually very similar to the CMOs in this case. The AdNDP results for Hg_4^{6-} embedded in the Na_3Hg_2 lattice do not differ significantly from the isolated Hg_4^{6-}: though the 4c-2e bonds for the embedded cluster were somewhat distorted in comparison to the isolated anion, the nodal patterns were the same. Another important observation from these results was that, though the Hg_4 cluster embedded in the crystalline lattice certainly did not carry charges of 6−, the aromaticity deciphered for the isolated Hg_4^{6-} cluster allowed one to understand why mercury atoms comprised a square-planar structure in the Na_3Hg_2 amalgam. Even though the isolated Hg_4^{6-} cluster was highly unstable against electron autodetachment, it existed in the amalgam due to the stabilizing environment of the sodium counter ions and more importantly the presence of aromaticity. Thus, the first solid compound containing the doubly aromatic all-metal cluster was identified.

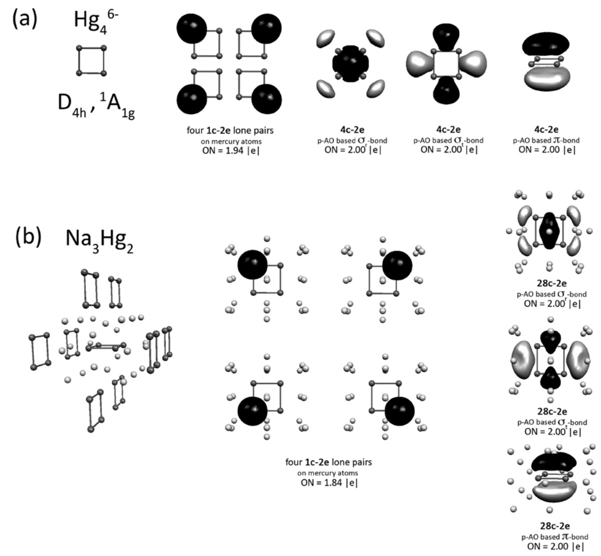

Fig. 4 The bonding elements recovered by AdNDP analyses for the isolated Hg_4^{6-} cluster (a); and for the Hg_4^{6-} cluster embedded in a part of the crystalline lattice of the Na_3Hg_2 amalgam comprised of 24 sodium cations placed at their position in the real crystalline structure (b).

Planar aromatic all-metal rings were also discovered in other solid compounds in 2004, when Todorov and Sevov reported synthesis of the new Zintl phases: Na_8BaPb_6, Na_8BaSn_6, and Na_8EuSn_6.[66] On the first glance at the chemical formula of those Zintl phases, one may think that the building block of those compounds should be either Pb_6 or Sn_6 clusters. Yet, it was shown by Todorov and Sevov that those phases contain isolated aromatic pentagonal rings of Sn_5^{6-} and Pb_5^{6-}, as well as isolated anions of Sn^{4-} and Pb^{4-}. The chemical bonding picture obtained by Sergeeva[14] using the AdNDP method for Sn_5^{6-} was the following: the 26 valence electrons of the Sn_5^{6-} clusters formed five 1c-2e lone pairs (one for each tin atom), five 2c-2e peripheral Sn–Sn σ-bonds, and three totally delocalized 5c-2e p-AO based π-bonds, satisfying the $4n + 2$ Huckel rule for aromaticity ($n = 1$). Thus, the aromaticity in the Sn_5^{6-} clusters was computationally confirmed. One can see that aromaticity discovered initially in isolated clusters was also established in solid compounds.

2.6. Li_3^+: an all-metal σ aromatic cluster

The double aromaticity discovered in Al_4^{2-}, Ga_4^{2-}, and Hg_4^{6-} suggested the possibility of metal clusters with σ-aromaticity only. Indeed, the Boldyrev lab showed[67] for the first time that the Li_3^+ cluster was the smallest all-metal σ-aromatic cluster with 2 delocalized σ electrons (Fig. 5).

The $1a_1'$-MO of Li_3^+ is a combination of the 2s-AOs of the three Li atoms (Fig. 5a), similar to the completely delocalized π-MO in $C_3H_3^+$, which consisted of $2p_z$-AOs of the C atoms (Fig. 5b). Analogous to the delocalized π-MO in $C_3H_3^+$, which renders its π-aromaticity according to the $4n + 2$ Hückel rule, the σ-delocalized MO in Li_3^+ renders its σ-aromaticity. This MO cannot be localized. An NBO analysis would produce a nonphysical picture with three lone pairs with an occupation number (ON) of 0.67 |e|. An AdNDP analysis confirmed that there was one 3c-2e bond in Li_3^+. The resonance energy (RE) was evaluated for the Li_3^+ cluster. Since it was more convenient to work with neutral species, the Li_3Cl neutral molecule, containing the Li_3^+ cation and a Cl^- counter ion, was studied. It was found to have a bidentate structure (C_{2v}, $^1A_1$)[67] with Cl^- coordinated to the edge of the Li_3^+ triangle, in agreement with a previous calculation.[68] The σ-RE in the Li_3^+ cation could be calculated as the energy of the following reaction:

$$Li_3Cl\ (C_{2v},\ ^1A_1) \rightarrow Li_2 + LiCl \qquad (1)$$

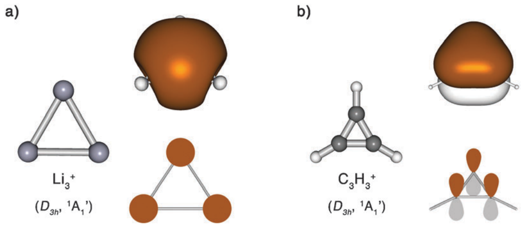

Fig. 5 (a) The structure of Li_3^+, its HOMO ($1a_1'$), and a representation of the HOMO as a linear combination of 2s-AOs of the Li atoms; (b) the structure of $C_3H_3^+$, its HOMO ($1a_2''$), and its representation as a linear combination of $2p_z$-AOs of C atoms. Here and elsewhere the lines between atoms do not necessarily represent the 2c-2e bonds.

Published on 28 January 2016. Downloaded by Brown University on 04/02/2017 04:05:37.

where Li_2 and LiCl were classical reference molecules (and could be represented by a single Lewis structure). The RE(Li_3^+) was found to be 36 kcal mol^{-1} (CCSD(T)/6-311+G(2df)//CCSD(T)/6-311+G*+ZPE/CCSD(T)/6-311+G*).[67] The calculated RE was very high compared to the Li_2 dissociation energy (23 kcal mol^{-1}). Another examples of σ-aromaticity were that in the Li_2Be_2 and other interesting molecules presented by Alexandrova.[67,69] One would expect that the classical linear Li–Be–Be–Li configuration would be the most stable structure for this cluster. However, it was found to be a cyclic structure, which was more stable by about 11 kcal mol^{-1}. In the cyclic structure, there were six delocalized σ-electrons, conforming to the $4n + 2$ rule for σ-aromaticity.

2.7. d-Orbital aromaticity

The all-metal aromatic clusters discussed above all composed of main group elements with either s- or p-AOs responsible for aromaticity. Transition metal atoms provided opportunities to discover aromaticity derived by d orbitals. The first d-orbital σ-aromaticity was observed in the $M_3O_9^-$ (M = W, Mo) clusters in 2005.[70] Simple electron counting in the $M_3O_9^-$ and $M_3O_9^{2-}$ clusters showed that if the oxidation state of oxygen was assumed to be 2− there were one and two extra electrons for direct metal–metal bonding in $M_3O_9^-$ and $M_3O_9^{2-}$, respectively. The singly and doubly charged anions were found to have high symmetry (D_{3h}) and the $^2A_1'$ and $^1A_1'$ electronic states, respectively, with two oxygen atoms coordinated to each M atom and three other oxygen atoms forming three M–O–M bridges in a cyclic structure. Analyses of the nature of the HOMOs in all anionic species revealed that they were all completely bonding three-center σ-bonds, thus rendering σ-aromaticity in these species. Since the delocalized HOMOs were formed from d-orbitals of transition metal atoms, these species were the first examples of d-orbital-based σ-aromatic molecules. The calculated NICS values at the center of $Mo_3O_9^{2-}$ (−21.5 ppm) and $W_3O_9^{2-}$ (−20.5 ppm), as well as estimated resonance energy for $W_3O_9^-$ of 7.6 kcal mol^{-1} supported the presence of aromaticity.[70]

Transition metal atoms also provided opportunities to find molecules with δ-aromaticity, where the delocalized orbitals were of δ-symmetry. The first example of a molecule exhibiting δ-aromaticity was reported in a joint photoelectron spectroscopic and theoretical study on the $Ta_3O_3^-$ cluster, which displayed three well-resolved photoelectron transitions in the low binding energy region.[71] Theoretical calculations showed that the $Ta_3O_3^-$ cluster had a closed-shell D_{3h} triangular global minimum structure. Comparison between the calculated and experimental VDEs confirmed the D_{3h} global minimum. Out of the 34 valence electrons in $Ta_3O_3^-$, 24 belonged to either pure oxygen lone pairs or those polarized towards the Ta atoms (responsible for the covalent contributions to the Ta–O bonding). The remaining 10 valence electrons were responsible for direct metal–metal bonding between the Ta atoms. The corresponding occupied MOs are shown in Fig. 6.

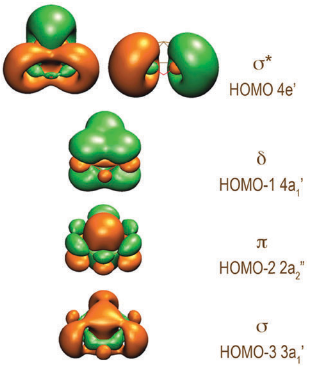

Fig. 6 The five valence MOs responsible for the metal–metal bonding in $Ta_3O_3^-$ (D_{3h}, $^1A_1'$). From ref. 71.

The doubly degenerate bonding/antibonding-HOMO (4e′) and the completely bonding HOMO−3 ($3a_1'$) were of σ-type. The bonding character of HOMO−3 was cancelled by the antibonding nature of the HOMO and thus the σ orbitals did not contribute significantly to direct metal–metal bonding. The HOMO−1 and HOMO−2 were completely bonding δ and π orbitals and, thus, this cluster was doubly (δ and π) aromatic according to the $4n + 2$ rule for aromaticity, with $n = 0$ applied separately to the δ and π systems. Detailed discussions on the δ-nature of the HOMO−1 can be found in ref. 52. Other examples of δ-aromaticity were found in the $Nb_3O_x^-$ (x = 0–8) clusters.[72–74] Recently, doubly σ and π aromaticity has been reported for the La_3^- cluster.[75] The Boldyrev group predicted the first cluster with triple σ-, π-, and δ-aromaticity.[76] It was shown that in the lowest singlet state of the Hf_3 cluster had a D_{3h} triangular shape with three 2c-2e Hf–Hf σ-bonds and three three-center delocalized bonds of the σ-, π-, and δ-type (Fig. 7), rendering triple aromaticity in this cluster.

There were comments that the δ-aromaticity would be too weak to be of value in chemistry. However, δ-aromaticity has been shown to be solely responsible for the stability of a transition metal cluster in a solid compound. Murahashi and co-workers[77] reported the synthesis of a remarkable $[Pd_4(\mu_4\text{-}C_9H_9)(\mu_4\text{-}C_8H_8)]^+$ triple-decker sandwich compound, in which the Pd_4^{2+} square cluster was sandwiched between an aromatic ($C_9H_9^-$) and an antiaromatic (C_8H_8) molecule. The Boldyrev group performed AdNDP analyses[78] on the bonding of the Pd_4^{2+} square cluster, as shown in Fig. 8.

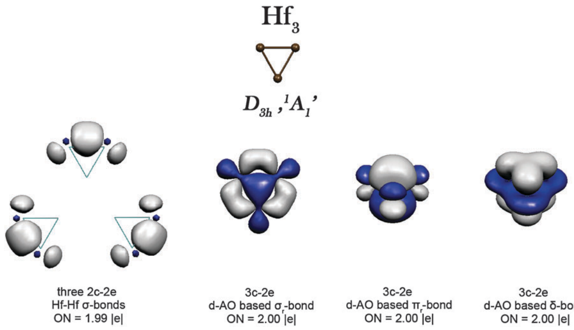

Fig. 7 The structure, three 2c-2e Hf–Hf σ-bonds, 3c-2e d-AO based σ_r-bonds, 3c-2e d-AO based π_r-bonds, and 3c-2e d-AO based δ-bonds revealed by the AdNDP analysis at B3LYP/LANL2DZ for the triply σ, π, and δ aromatic Hf_3 cluster.

Published on 28 January 2016. Downloaded by Brown University on 04/02/2017 04:05:37.

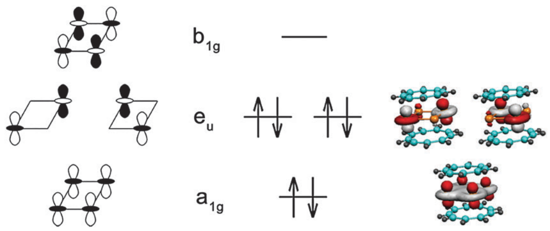

Fig. 8 The d-bonding in the Pd$_4^{2+}$ cluster in the [Pd$_4$(μ$_4$-C$_9$H$_9$)(μ$_4$-C$_8$H$_8$)]$^+$ complex.

The AdNDP analysis revealed four lone pairs on each Pd atom based on 4d AOs (not shown in Fig. 8) and three 4c-2e d-orbitals (Fig. 8), which were solely responsible for the Pd–Pd bonding, rendering it δ-aromaticity. Thus, the [Pd$_4$(μ$_4$-C$_9$H$_9$)(μ$_4$-C$_8$H$_8$)]$^+$ compound could be viewed as the first synthesized compound in the solid state with δ-aromaticity. Even though δ-aromaticity is admittedly weaker than σ- and π-aromaticity, it can play an important role in chemistry.

Recently, d-orbital aromaticity has been found in a number of inorganic solid compounds, *e.g.*, the aromatic Pd$_3^+$ ring in the [{(SAr′)(PAr$_3$)Pd}$_3$]$^+$ complex,[79] the aromatic [ZnBi$_4$]$^{3-}$ pentagon in the K$_6$ZnBi$_5$ compound,[80] the aromatic Au$_3^+$ ring in the [(IPrAu)$_3$]$^+$ cation,[81] and aromatic [Zn$_3$]$^+$ and [Zn$_2$Cu] clusters in simple compounds.[82]

2.8. All-metal 3D aromaticity

In 2002 we also uncovered a few examples of all-metal three-dimensional aromaticity.[83] The Wang lab made a series of MAl$_6^-$ (M = Li, Na, K, Cu, and Au) bimetallic clusters in a supersonic cluster beam and obtained their photoelectron spectra. Computational searches for the global minimum structures by the Boldyrev lab revealed that the most stable structure for these clusters contained a somewhat distorted octahedral Al$_6^{2-}$ unit with an M$^+$ ion coordinated to one of the faces of the octahedron. Comparisons between the computed and experimental VDEs confirmed these global minimum structures. The electron configuration for an isolated perfectly octahedral Al$_6^{2-}$ gave the following electron configuration: $1a_{1g}^2 1t_{1u}^6 1e_g^4 1t_{2g}^6 2a_{1g}^2$. The six lowest CMOs could be localized into six lone pairs (one on each Al atom), but the next four orbitals (1t$_{2g}$ and 2a$_{1g}$) were completely delocalized over the whole Al$_6^{2-}$ cluster. The eight delocalized bonding electrons satisfy the $2(n+1)^2$ counting rule for three-dimensional aromaticity ($n = 1$ in this case).[84] Since then, an all-metal spherical aromatic molecule has been found in the solid state. Li and co-workers reported two remarkable $\{[\mathrm{Mn}^{\mathrm{I}}_8\mathrm{Mn}^{\mathrm{II}}_3(\mathrm{H_2O})_6(\mathrm{HL})_{12}](\mathrm{OH})_2\cdot17\mathrm{H_2O}\}_n$ (L = tetrazole dianion) and $[\mathrm{Zn}^{\mathrm{I}}_8(\mathrm{HL})_4(\mathrm{L})_8]^{12-}$ (L = tetrazole dianion) cluster compounds,[85,86] which featured the first example of cubic aromaticity. The example of spherical aromaticity due to d-orbitals was also demonstrated in the Ce$_6$O$_8$ cluster.[87]

It should be pointed out that extension of the jellium model has led to the concept of superatoms that can explain the stability of gold nanoclusters.[88] The jellium model is also based on the idea of electron delocalization and is more appropriate for large systems. For small clusters with well-defined geometrical structures, the aromaticity concept is more suitable. The 3D-aromaticity for large clusters should be similar to the superatom concept, which would be interesting to be investigated in the future.

3. Aromaticity in size-selected boron clusters

Joint photoelectron spectroscopy and theoretical studies over the past decade have allowed the structures and bonding of size-selected boron clusters to be systematically elucidated up to 27 atoms, as shown in Fig. 9. All these cluster anions have planar or quasi-planar (2D) global minima, which were confirmed by comparison between experimental photoelectron spectra and computed VDEs. Several reviews have appeared about these research efforts.[10,89–91] In particular, a brief account of the chemical bonding and structural fluxionality of boron clusters up to B$_{24}^-$ has appeared in 2014.[90] While there is some overlap with the previous account, the current Perspective focuses on the aromaticity of the planar boron clusters with a few selected examples. Specifically, major progress has been made since the last account in solving the structures of several large boron clusters, including the planar hexagonal B$_{36}$ and B$_{35}^-$ and the discoveries of borophenes and borospherenes (see Sections 3.5 and 3.6).

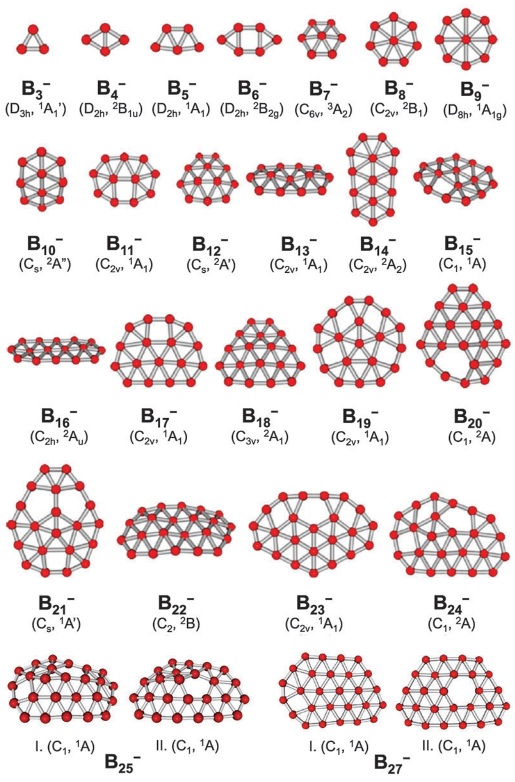

Fig. 9 A summary of the global minima of B$_n^-$ (n = 3–25, 27) clusters confirmed by experiment.[83] Note that a close-lying isomer is also shown for B$_{25}^-$ and B$_{27}^-$.

View Article Online

Published on 28 January 2016. Downloaded by Brown University on 04/02/2017 04:05:37.

The chemical bonding in these planar boron clusters is interesting. The B–B bonds on the periphery of each cluster are classical 2c-2e σ bonds, whereas the bonding between the interior atoms and the periphery ($n \geq 7$) or between the interior atoms ($n \geq 10$) is all delocalized, as a result of boron's electron deficiency. There are both delocalized σ and π bonds, giving rise to concepts of σ and π aromaticity/antiaromaticity, multiple aromaticity or even conflicting aromaticity. More interestingly, the delocalized π bonding in most planar boron clusters has been found to be analogous to those in PAHs, giving rise to the concept of hydrocarbon analogues of boron clusters.

3.1. The B_9^- cluster: a prototypical planar boron cluster with doubly σ and π aromaticity

The σ and π aromaticity of planar boron clusters can be best illustrated by the B_9^- cluster, which was among one of the earliest boron clusters to be elucidated collaboratively by the Boldyrev and Wang groups.[92] It possesses a perfectly planar wheel structure with D_{8h} symmetry (Fig. 9). As shown in Fig. 10, among its twenty eight valence electrons, sixteen are used to form eight peripheral 2c-2e bonds, the remaining twelve electrons form three completely delocalized 9c-2e σ and three 9c-2e π bonds. The delocalized π bonds of B_9^- are very similar to those in benzene and the number of π electrons obeys the $4n + 2$ Huckel rule, rendering it π aromatic. The delocalized σ bonds are very similar to the π bonds, giving rise to σ aromaticity in B_9^-. The delocalized σ and π bonds together make B_9^- doubly aromatic, consistent with its high electronic stability. The B_8 cluster with a similar wheel structure (D_{7h}) was found to have a similar electronic structure with two unpaired electrons, even though the B_8^- anion was found to have C_{2v} symmetry (Fig. 9) due to the Jahn–Teller effect.[92] The closed-shell B_8^{2-} had exactly the same double aromaticity as B_9^- with six delocalized σ and six delocalized π electrons.

Further studies showed that B_{10}, B_{11}^-, and B_{12} all had six delocalized π electrons and were aromatic according to the $4n + 2$ Huckel rule.[93] However, B_{13}^- and B_{14} each had eight delocalized π electrons and were antiaromatic according to the $4n$ rule. The antiaromaticity in these two clusters was consistent with their elongated structures (Fig. 9). The B_{15}^- cluster was shown to have ten π electrons and was again aromatic, in agreement with its more circular structure. It is interesting to point out that the B_{13}^+ cluster had a more circular structure,[94] different from the more elongated B_{13}^- structure. Fowler and Ugalde first analyzed the electronic structure of the planar B_{13}^+ (six π electrons) and recognized the possibility of Huckel aromaticity.[95] Hence, there is a close relationship between aromaticity/antiaromaticity and the global structures of planar boron clusters.

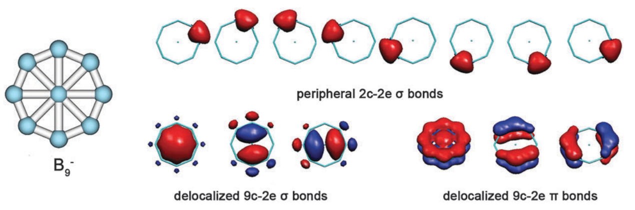

Fig. 10 AdNDP analyses of the bonding in the D_{8h} global minimum of the B_9^- cluster.[60]

3.2. B_{16}^-: an all-boron naphthalene

The global minimum of B_{16}^- was found to be an elongated quasi-planar structure with C_{2h} symmetry (I.1 in Fig. 11). The quasi-planarity came from the fact that the four inner B atoms exhibited a zigzag pattern with an out-of-plane distortion of 0.08 Å.[95] The global minimum of neutral B_{16} was found to be similar to that of B_{16}^-, but with more out-of-plane distortions by 0.24 Å (II.1 in Fig. 11). The anion structure was confirmed by comparison with photoelectron spectroscopy,[96] whereas the neutral B_{16} structure was confirmed by infrared spectroscopy.[97] For B_{16}^+, the ion mobility experiment suggested a double ring structure,[98] which was a much higher energy isomer for B_{16}^- and B_{16}. The global minimum of B_{16}^- was an open-shell species with a doublet electronic state (^2A_u). It was found that addition of an electron to B_{16}^- resulted in a perfect planar and closed-shell B_{16}^{2-} dianion (D_{2h}, ^1A_g) (III.1 in Fig. 11).

Chemical bonding analyses showed that the D_{2h} B_{16}^{2-} dianion possessed ten π electrons, analogous to the well-known aromatic naphthalene, as shown in Fig. 12. Thus, B_{16}^{2-} was considered to be an "all-boron naphthalene".[96] The removal of two electrons from the HOMO of B_{16}^{2-} led to the neutral B_{16} cluster with eight π electrons, *i.e.* an antiaromatic system according to the $4n$ rule, which explained the significant out-of-plane distortions in B_{16}. The B_{16}^- anion with seven π electrons had an out-of-plane distortion in between the perfectly planar B_{16}^{2-} and neutral B_{16}.

The B_{17}^- cluster was found to have a planar C_{2v} structure with five delocalized π MOs,[99] very similar to those found in B_{16}^{2-}. Hence, B_{17}^- was another all-boron analogue of naphthalene.

3.3. B_{19}^-: concentric double π aromaticity

The global minimum of the B_{19}^- cluster was confirmed to be a spider-web-like structure (I in Fig. 13),[100] which was almost perfectly circular with one boron atom at the center surrounded

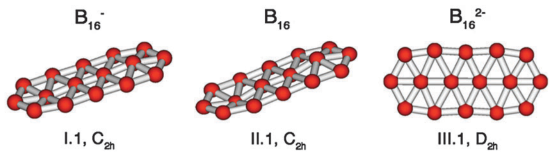

Fig. 11 The global minima of B_{16}^- (^2A_g), B_{16} (^1A_g), and B_{16}^{2-} (^1A_g).[96]

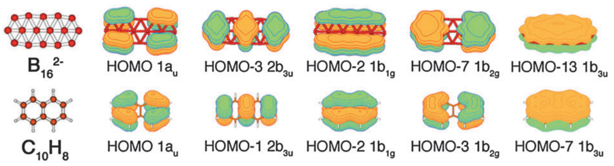

Fig. 12 Comparison of the occupied π MOs of B_{16}^{2-} with those of naphthalene.[96]

Published on 28 January 2016. Downloaded by Brown University on 04/02/2017 04:05:37.

by five boron atoms and a peripheral ring of thirteen atoms. Another planar isomer with a triangular B_6 in the center (II in Fig. 16) was found to be quite low-lying, 1.75 kcal mol^{-1} at B3LYP and 3.73 kcal mol^{-1} at the CCSD(T) level of theory above the global minimum. An elongated isomer (III in Fig. 13) and a double ring isomer (IV in Fig. 13) were found to be much higher in energy.

MO analyses for the global minimum of B_{19}^- (Fig. 14b) showed the similarity of its π bonding to that in the [10]annulene molecule (Fig. 14a), except that B_{19}^- had one extra π MO. Close examination found that a linear combination of the HOMO and HOMO−15 would generate one MO delocalized between the B_5 ring and the outer ring and another MO delocalized over the inner filled pentagon. Hence, B_{19}^- consisted of two concentric delocalized π systems: one between the B_5 ring and the outer B_{13} ring with five π MOs, which were analogous to the π system in the [10]annulene, and another single π MO delocalized over the central filled pentagon. AdNDP analyses (Fig. 14c) showed more clearly the two π systems. Each of the two π systems obeyed the $4n + 2$ Huckel rule. Thus, the B_{19}^- cluster was considered to be a concentric doubly π aromatic species.

The low-lying isomer II of B_{19}^- (Fig. 13), which could have made minor contributions to the experimental photoelectron spectra, was also found to be doubly π aromatic with a similar concentric π system to isomer I. The key structural difference between the two isomers was the arrangement of the central B_6 unit. In the global minimum isomer I, the B_6 unit was a filled pentagon with near D_{5h} symmetry, resulting in its near circular structure, whereas in isomer II the six interior B atoms formed a triangle, giving rise to the overall triangular shape of this isomer.

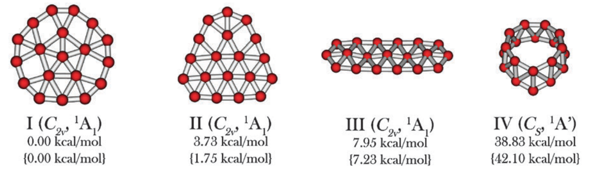

Fig. 13 The global minimum and three low-lying isomers of B_{19}^-. The relative energies of the higher-lying isomers are given at the CCSD(T) and B3LYP (in curly brackets) levels of theory.[100]

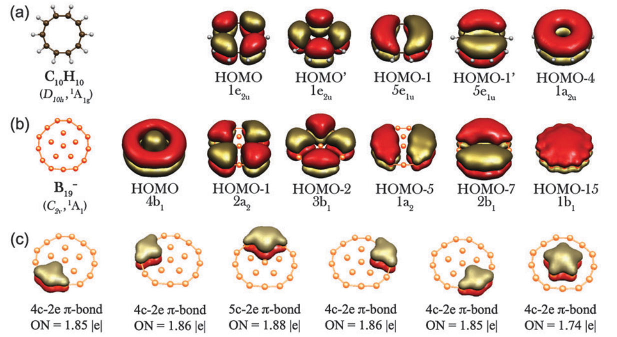

Fig. 14 Comparison of the π MOs of [10]annulene (a) with those of the global minimum of B_{19}^- (b). (c) AdNDP analyses of the π bonding in B_{19}^-, showing that five π bonds are delocalized between the inner B_5 ring and the outer B_{13} ring similar to those in [10]annulene and one π bond delocalized over the inner filled pentagon.[100]

The concentric double π aromaticity in the global minimum of B_{19}^- has interesting dynamic consequences. Using molecular dynamic simulations, Merino and co-workers found that the inner filled pentagon could freely rotate at finite temperatures against the outer B_{13} ring and proposed B_{19}^- as a molecular Wankel motor.[101]

Two nearly degenerate structures were found to compete for the global minimum for the B_{18}^- cluster.[99] These two structures were related to the two low-lying isomers of B_{19}^- (I and II in Fig. 13) by removing a peripheral B atom, respectively. Because of the reduced periphery, both structures of B_{18}^- experienced out-of-plane distortions with a bowl shape. In particular, the B_{18}^{2-} species was found to have the same number of π electrons as the corresponding B_{19}^- cluster and both were doubly π aromatic with two concentric π systems. Merino and co-workers also found that the inner filled pentagon in the bowl-shaped B_{18}^{2-} could undergo hindered rotation against the B_{12} periphery, making it a member of the molecular Wankel motor family.[102]

3.4. B_{23}^-: an all-boron phenanthrene

Global minimum searches for large boron clusters ($n > 20$) were quite challenging.[91] Following the solution of the B_{21}^- cluster,[103] the Boldyrev and Wang groups jointly investigated the B_{22}^- and B_{23}^- clusters in 2012.[104] Both clusters were found to have 2D structures with their π bonding analogous to PAHs. The first five isomers of B_{23}^- are shown in Fig. 15 at two levels of theory. A beautiful heart-shaped planar structure with a pentagonal hole was found to be the global minimum. The second isomer consisted of a buckled triangular lattice, but was significantly higher in energy. The other three isomers were much higher in energy, including the tubular isomer V in Fig. 15. The calculated VDEs of the heart-shaped global minimum were found to be in excellent agreement with the experimental photoelectron spectra. The VDEs of isomer II were also computed, but they disagreed with the experiment. The heart-shaped B_{23}^- was particularly stable and was the only contributor to the observed photoelectron spectrum, confirming firmly that it was the global minimum of B_{23}^-.

Chemical bonding analyses for the B_{23}^- "nanoheart" revealed seven π orbitals, which were found to be identical to those of phenanthrene, as shown in Fig. 16. Thus, B_{23}^- could be considered to be an all-boron phenanthrene.[104] In addition to the seven delocalized π bonds, AdNDP analyses showed that B_{23}^- consisted of fifteen localized 2c-2e σ bonds on the periphery and thirteen delocalized σ bonds in the interior of

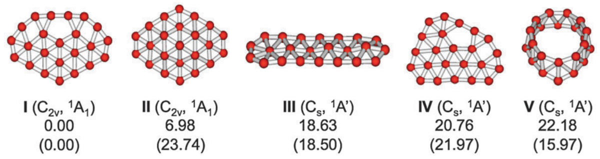

Fig. 15 The global minimum and low-lying isomers of B_{23}^- at the PBE1PBe and B3LYP (in parentheses) levels of theory.[104]

Published on 28 January 2016. Downloaded by Brown University on 04/02/2017 04:05:37.

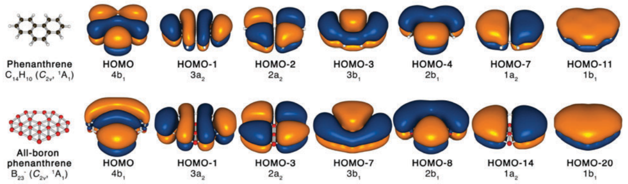

Fig. 16 Comparison of the π MOs of B_{23}^- with those of phenanthrene.[103]

the 2D plane. The aromaticity played a major role in stabilizing the B_{23}^- nanoheart. A heart-shaped B_{23}^+ cation would lose two π electrons in the HOMO and become π antiaromatic, thus much less stable. Indeed, the global minimum of the B_{23}^+ cation was shown to be something similar to isomer II (Fig. 15), but distorted to C_2 symmetry, at the TPSS level of theory,[98] though the ion mobility data were in better agreement with a higher energy, low symmetry tubular structure.

The B_{22}^- cluster was found to have a planar global minimum structure with a buckled triangular lattice. Chemical bonding analyses on the closed-shell B_{22}^{2-} species also revealed seven occupied π orbitals, similar to those found for B_{23}^- (Fig. 16). Remarkably, the π MOs in B_{22}^{2-} were found to be similar to the π orbitals of anthracene, an isomer of phenanthrene, with three connected benzene rings in a row.[104] Hence, B_{22}^{2-} could be considered to be an all-boron anthracene.

3.5. B_{36}^-: an all-boron coronene

The B_{36}^- cluster was observed to give a well-resolved photoelectron spectrum with an unusually low electron binding energy in a preliminary study as early as 2005.[91] But its structure was not solved until 2014,[105] due to the challenges of global minimum searches. Extensive global minimum searches using two different methods found that the most stable isomer of B_{36}^- had a 2D structure with a central hexagonal hole, as shown in Fig. 17a (isomer I), where a tubular isomer (II) and a planar isomer with a double hole (III) were also given. Most importantly, only the simulated spectrum of the hexagonal structure agreed with the observed photoelectron spectrum. The global minimum of B_{36}^- was open-shell and had C_{2v} symmetry because of the Jahn–Teller effect. The neutral closed-shell B_{36} was shown to have a perfect hexagonal symmetry (C_{6v}), albeit with a slight out-of-plane distortion (I^0 in Fig. 17b). The hexagonal structure was found to be much more stable than either the tubular isomer (II^0) or the planar isomer with a double hole (III^0).

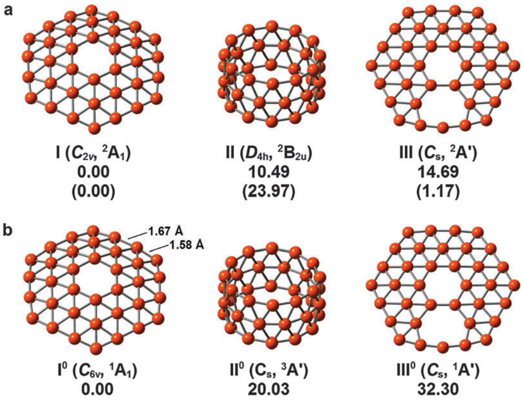

Fig. 17 The global minimum and low-lying isomers of B_{36}^- (a) and B_{36} (b).[105]

The results of chemical bonding analyses for the C_{6v} B_{36} using AdNDP are shown in Fig. 18. Because the peripheral bonds were not equivalent (Fig. 17b), twelve 2c-2e peripheral σ bonds were found (Fig. 18a) and the six slightly longer peripheral bonds were found to involve in 3c-2e σ bonds (Fig. 18b). The inner B_6 hexagon was also found to involve in six 3c-2e σ bonds (Fig. 18b). There were eighteen 4c-2e σ bonds (Fig. 18c), which suggested that the B_{36} cluster could be viewed as consisting of six filled hexagonal B_7 (B@B_6) units. The π bonding patterns were also very interesting. There were six 4c-2e π bonds on the outer part of the B_{36} cluster (Fig. 18d) and six globally delocalized 36c-2e π bonds (Fig. 18e).

Because the AdNDP analyses did not give unique solutions for the bonding pattern,[60] Chen *et al.* found a beautiful analogy of the π bonding pattern of B_{36} to that of coronene with slightly lower occupation numbers,[106] extending the PAH analogy of 2D boron clusters to a very large system. They obtained similar σ bonding patterns as shown in Fig. 18, as well as six 4c-2e π bonds similar to those in Fig. 18d. However, they were able to partition the six 36c-2e bonds into two sets with slightly lower occupation numbers: one set was mainly delocalized between the central B_6 ring and the middle B_{12} ring and another set was mainly delocalized between the outer B_{18} ring and the middle B_{12} ring, which were found to be analogous to the delocalized π bonding pattern in coronene, as schematically shown in Fig. 19.

The B_{36} cluster was the smallest boron cluster to display hexagonal symmetry. A planarized B_{36} can be used to "construct" extended atom-thin boron sheets with hexagonal holes, which were called "borophenes",[105] in analogy to graphene. Due to the electron deficiency of boron, it cannot form an extended

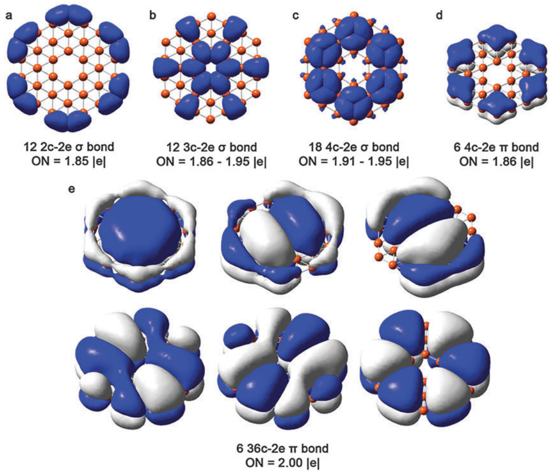

Fig. 18 AdNDP analyses of the chemical bonding in the global minimum of B_{36}.[105] ON indicates the occupation number.

This journal is © the Owner Societies 2016

Published on 28 January 2016. Downloaded by Brown University on 04/02/2017 04:05:37.

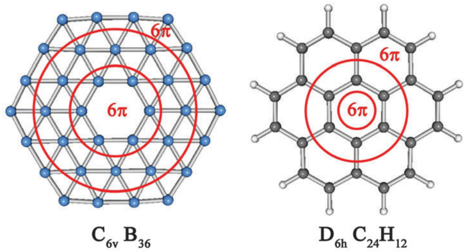

Fig. 19 Schematic comparison between the π bonding patterns of B_{36} and coronene.

graphene-like hexagonal lattice. However, theoretical calculations showed that extended graphene-like boron-monolayers with partially filled hexagons or extended triangular lattices with hexagonal holes were highly stable.[107,108] The stability of the hexagonal B_{36} cluster provided indirect experimental evidence for the viability of such boron nanostructures.

3.6. B_{35}^-: an all-boron benzo(*g*,*h*,*i*)perylene ($C_{22}H_{12}$)

The photoelectron spectrum of B_{35}^- (Fig. 20a) was found to display features similar to that of B_{36}^-, suggesting that their structures might be related.[109] Global minimum searches indeed led to a structure of B_{35}^-, which could be viewed as removing a B atom from the middle B_{12} ring of B_{36} (Fig. 20b). The global minimum of B_{35}^- featured two hexagonal holes adjacent to each other with little other geometrical change relative to the hexagonal B_{36}. Most importantly, the simulated spectrum of this B_{35}^- structure was almost in perfect agreement with the experiment (Fig. 20b).

Chemical bonding analyses for B_{35}^- using AdNDP are shown in Fig. 21a, featuring eighteen localized 2c-2e peripheral σ bonds and a localized interior 2c–2e σ bond between the two hexagonal holes. A similar localized interior 2c-2e σ bond was observed in B_{21}^- between its two pentagonal holes.[103] In addition, there were twenty-three delocalized σ bonds and eleven delocalized π bonds. The π bonding in B_{35}^- was found to be analogous to that in the benzo(*g*,*h*,*i*)perylene PAH molecule ($C_{22}H_{12}$), as shown in Fig. 21b.

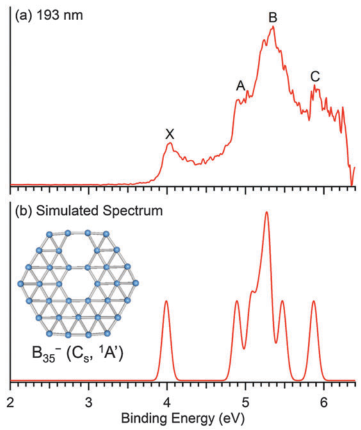

Fig. 20 The photoelectron spectrum of B_{35}^- at 193 nm (a), compared with the simulated spectrum of the global minimum of B_{35}^- (b).[109]

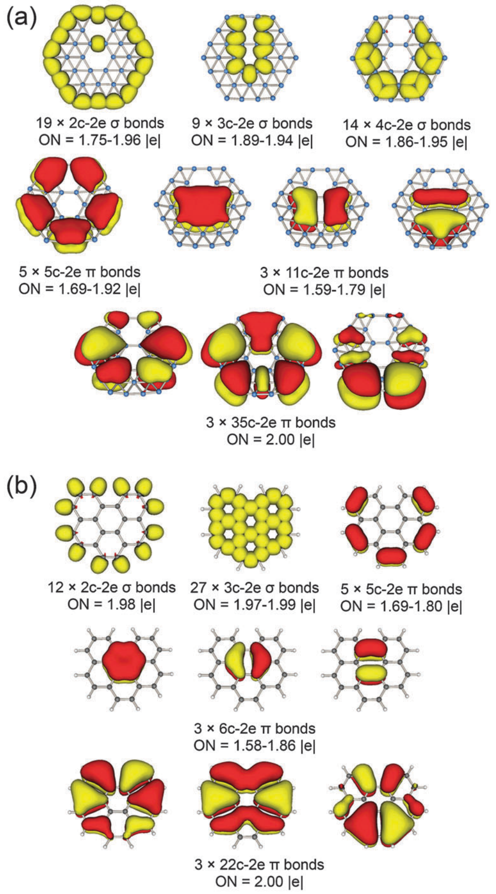

Fig. 21 Comparison of chemical bonding of B_{35}^- with that of the $C_{22}H_{12}$ PAH molecule using AdNDP analyses.[109] Note the similarity in π bonding in the two systems. ON indicates the occupation number.

The central hexagonal hole in the C_{6v} B_{36} was critical for its 2D structure. The slight out-of-plane distortion was really due to the peripheral effect, *i.e.*, the peripheral B–B bonds tend to be stronger or slightly shorter than the interior B–B bonds. It was interesting to note that the second hexagonal hole in B_{35}^- induced very little structural distortion and in fact made the cluster slightly more planar, reinforcing the importance of hexagonal vacancies in the stabilization of borophenes. Monolayer boron sheets with different hexagonal hole densities and patterns were further considered theoretically.[110,111] It was found that the planar B_{35} cluster was in fact a more flexible motif to construct borophenes with adjacent hexagonal holes or mixed hexagonal holes.[109]

The B_{40} cluster was discovered to be the first all-boron fullerene, called borospherene, which was a highly stable electronic system with D_{2d} symmetry and a large HOMO–LUMO gap.[112] However, in the B_{40}^- anion, a planar isomer with a double hexagonal hole similar to that in B_{35}^- with C_s symmetry was found to be slightly more stable than the D_{2d} borospherene and both co-existed experimentally.[112] The C_s B_{40}^- had a very high electron binding energy and in fact the closed-shell C_s B_{40}^{2-} was found to be electronically stable as a dianion. Chemical bonding analyses showed that the π bonding pattern

Published on 28 January 2016. Downloaded by Brown University on 04/02/2017 04:05:37.

in the C_s B_{40}^{2-} was similar to that in the closed-shell $C_{27}H_{23}^+$ PHA molecular ion,[113] extending the hydrocarbon analogy of boron clusters to the largest size thus far.[91]

4. Designing aromatic borometallic molecular wheels ($M@B_n^-$, n = 8–10)

4.1. Design principle based on σ and π double aromaticity

As seen above, aromaticity plays a central role in providing electronic stability to 2D boron clusters. The bonding for all interior atoms is delocalized both in the σ and π frameworks, except for a few cases, such as B_{21}^- or B_{35}^- (Fig. 21a), where two boron atoms are shared by two defects (*i.e.* non-triangles). Hence, the valence electrons for the interior boron atoms all participate in delocalized bonding. For example, in the D_{8h} B_9^- cluster (Fig. 9), each peripheral B atom forms two localized B–B bonds with its neighboring peripheral B atoms and contributes its third valence electron to the delocalized bonding with the central B atom. The central B atom, on the other hand, contributes all its three valence electrons to delocalized bonding. Thus, there are twelve delocalized electrons in B_9^-, six for the delocalized σ bonds and six for the delocalized π bonds, resulting in the doubly σ and π aromaticity, as shown in Fig. 10. The double aromaticity of B_9^- provides high electronic stability for this beautiful wheel-like cluster.

The electronic structure and bonding of B_9^- inspired us to substitute the central B atom in B_9^- by a metal atom to create metal-centered molecular wheels, because metal atoms are even better electron donors and more willing partners for delocalized bonds. We have proposed an electronic design principle for metal-centered boron wheels with different ring sizes, $M@B_n^{k-}$. If we assume that the valence of M is x, then the total number of valence electrons in the system is $x + 3n + k$. For a stable $M@B_n^{k-}$ wheel with double aromaticity, we need 12 electrons for the delocalized σ and π bonding and $2n$ electrons for the peripheral localized B–B bonds, *i.e.*, $x + 3n + k = 2n + 12$, or

$$x + n + k = 12 \qquad (2)$$

If the valence of M and the ring size satisfy this equation, we expect a stable electronic system with double aromaticity. Based on this design principle, we have made and characterized a series of transition metal centered molecular wheels for n = 8–10.[114–117] It turned out that the geometrical constraint is also important. If the ring size is too small, there is not enough room for the central M atom.[118,119] If the ring size is too large, the M–B bonding would not be favorable and the wheel structures cannot compete with other 3D structures.[120,121] More interestingly, we found that main group elements, such as Al, do not favor the central position[122–124] and no molecular wheels with any main group metals have been observed experimentally, even though some main group systems were considered computationally.[125,126] A brief account of this research has appeared previously.[127] A few examples will be discussed in this Perspective, highlighting the importance of aromaticity in these novel borometallic molecular wheels, which may be subjects of large-scale laboratory syntheses if appropriate ligands can be found to coordinate axially to the central transition metal atoms.

4.2. $M@B_8^-$: molecular wheels with eight-membered rings

The first metal-centered molecular wheel was the $Co@B_8^-$ cluster,[114] which was produced by the laser vaporization of a B/Co composite target. It gave relatively simple photoelectron spectra with vibrational resolution and very high electron binding energies, suggesting a high symmetry cluster and a very stable electronic system. Theoretical calculations showed that $Co@B_8^-$ had a perfect D_{8h} wheel structure (Fig. 22). The calculated VDEs for the $Co@B_8^-$ wheel were in good agreement with the experimental photoelectron spectra. The neutral $Co@B_8$ cluster also had a planar wheel structure, but slightly distorted to D_{2d} symmetry due to the Jahn–Teller effect (Fig. 22). The resolved vibrational structures were consistent with the structural changes between the anion and neutral.

According to our electronic design principle of eqn (2), the Co atom in $Co@B_8^-$ should be valent III and contribute three electrons to the delocalized bonding between Co and the B_8 ring. This was exactly what we found from chemical bonding analyses using both MOs and AdNDP (Fig. 23). The AdNDP analyses revealed three pairs of 3d electrons, implying that Co is in its 3+ oxidation state. In addition, eight 2c-2e B–B bonds, three delocalized σ bonds, and three delocalized π bonds were found, exactly as anticipated from our design principle.

We have also found $Fe@B_8^-$ to have a molecular wheel structure, in which Fe is in its 3+ oxidation state.[117] However, $Fe@B_8^-$ has a C_{8v} structure with the Fe atom slightly out of plane, due to a second order Jahn–Teller effect, because $Fe@B_8^-$ is an open-shell with an unpaired electron in the Fe $3d_{z^2}$ orbital.

4.3. $M@B_9^-$: molecular wheels with nine-membered rings

The first metal-centered molecular wheel found with a nine membered ring was the $Ru@B_9^-$ cluster.[114] This cluster also gave

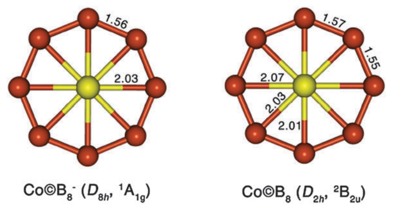

Fig. 22 The optimized structures of $Co@B_8^-$ and $Co@B_8$ molecular wheels.[114]

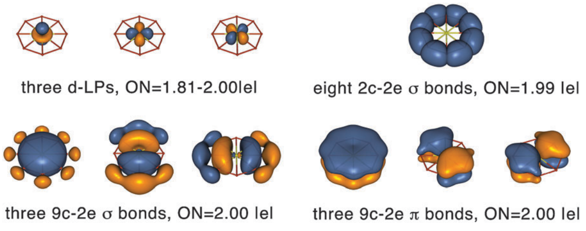

Fig. 23 AdNDP analyses for the D_{8h} $Co@B_8^-$ molecular wheel.[114]

Published on 28 January 2016. Downloaded by Brown University on 04/02/2017 04:05:37.

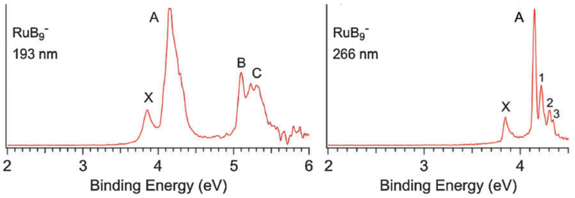

Fig. 24 Photoelectron spectra of Ru@B$_9^-$ at two photon energies. The numbers in the 266 nm spectrum indicate the vibrational structures.[114]

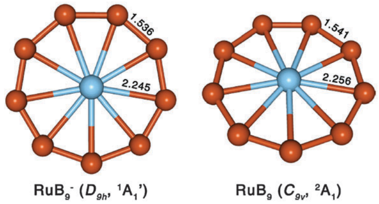

Fig. 25 The optimized structures of Ru@B$_9^-$ and Ru@B$_9$ molecular wheels.[114]

a simple photoelectron spectral pattern with high electron binding energies and vibrational resolution (Fig. 24), again suggesting a high symmetry structure and a stable electronic system. According to the electronic design principle of eqn (2), the valence of Ru in Ru@B$_9^-$ should be 2+. Structural searches indeed found a perfectly planar D_{9h} Ru@B$_9^-$ molecular wheel with a closed electronic shell, as shown in Fig. 25. The computed VDEs of the D_{9h} Ru@B$_9^-$ wheel were in good agreement with the experimental spectra. The neutral Ru@B$_9$ cluster was found to have C_{9v} symmetry with the Ru atom only very slightly out-of-plane, again due to a second order Jahn–Teller effect.

Chemical bonding analyses using AdNDP for Ru@B$_9^-$ are shown in Fig. 26. The bonding is quite similar to that in Co@B$_8^-$, except there are nine 2c-2e B–B σ bonds. The three d lone pairs indicate that Ru is in its 2+ oxidation state, as predicted by the design principle of eqn (2). The delocalized σ and π bonds for double aromaticity are nearly identical to those in Co@B$_8^-$.

The Fe@B$_9^-$ cluster was also found to be a molecular wheel with nearly identical structure and bonding as the isoelectronic Ru@B$_9^-$ cluster.[117] Neutral nine-membered molecular wheels have been found in Rh@B$_9$ and Ir@B$_9$, which are closed-shells with D_{9h} symmetry.[115] According to the design principle, the Rh and Ir atoms are in their 3+ oxidation state. Chemical bonding analyses by AdNDP revealed very similar bonding to that in the D_{9h} Ru@B$_9^-$ cluster.

Fig. 26 AdNDP analyses for the D_{9h} Ru@B$_9^-$ molecular wheel.[114]

The V@B$_9^{2-}$ species was also found to be a perfectly D_{9h} molecular wheel.[118] However, in this case, the design principle needed to be modified, because its double aromaticity was derived from six delocalized π electrons and ten delocalized σ electrons, *i.e.*, in this case, the design principle should be modified as:

$$x + n + k = 16 \qquad (3)$$

This modified design principle was first realized in the ten-membered-ring molecular wheels, Ta@B$_{10}^-$ and Nb@B$_{10}^-$,[116] as will be discussed below. However, the Nb@B$_9^{2-}$ and Ta@B$_9^{2-}$ species, isoelectronic with V@B$_9^{2-}$, were found to have C_{9v} symmetry, because of the geometric constraint, even though they obeyed the modified electronic design principle expressed in eqn (3). The B$_9$ ring was simply too small to host the larger Nb and Ta atoms in Nb@B$_9^{2-}$ and Ta@B$_9^{2-}$.[118]

4.4. M@B$_{10}^-$: molecular wheels with ten-membered rings

According to the electronic design principle of eqn (2), an M@B$_{10}^-$ molecular wheel with double aromaticity would require the central metal atom to be a valence I element. The most promising atom would be Au, considering the size requirement. However, Au was found to bond with boron clusters like a hydrogen atom.[128,129] The AuB$_{10}^-$ cluster was found to have a structure, in which the Au atom was covalently bonded to the periphery of a planar B$_{10}^-$ cluster,[130] while the D_{10h} Au@B$_{10}^-$ wheel structure was a much higher energy isomer. Hence, the interactions between the d orbitals in the central atom and the boron ring played a significant role in stabilizing the molecular wheels.

Experimentation with different metal atoms led to the observation of very simple photoelectron spectra for TaB$_{10}^-$ with very high electron binding energies (Fig. 27a and b), suggesting a high symmetry and stable electronic system. The photoelectron spectra of the isoelectronic NbB$_{10}^-$ (Fig. 27c and d), however, revealed a more complicated picture. In addition to photoelectron features similar to those of TaB$_{10}^-$, the spectra of NbB$_{10}^-$ also contained weak signals in the low binding energy region.

Theoretical calculations found that the TaB$_{10}^-$ cluster had a D_{10h} Ta@B$_{10}^-$ global minimum with a higher lying 3D isomer,

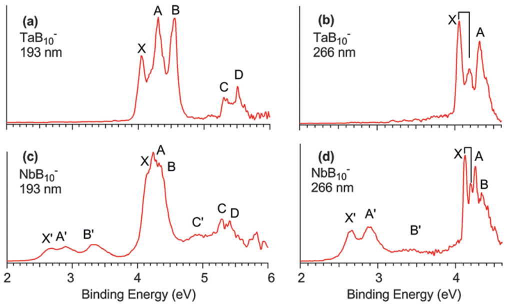

Fig. 27 Photoelectron spectra of TaB$_{10}^-$ at 193 nm (a) and 266 nm (b) and NbB$_{10}^-$ at 193 nm (c) and 266 nm (d). The vertical lines in the 266 nm spectra indicate the vibrational structures for band X.[116]

Published on 28 January 2016. Downloaded by Brown University on 04/02/2017 04:05:37.

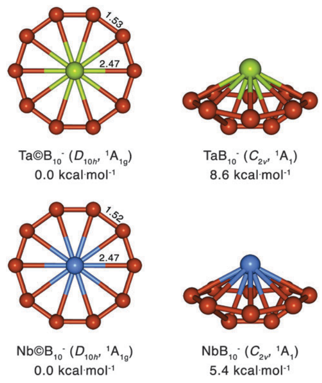

Fig. 28 The optimized global minimum wheel structures of Ta@B$_{10}^-$ and Nb@B$_{10}^-$ and a low-lying 3D isomer.[116]

as shown in Fig. 28. The simulated spectrum of the Ta@B$_{10}^-$ molecular wheel was in good agreement with the observed photoelectron spectra. For NbB$_{10}^-$, theoretical calculations also found the D_{10h} molecular wheel to be the global minimum, but the corresponding 3D isomer was much lower-lying (Fig. 28) and could be accessible experimentally at finite temperatures. Indeed, the computed VDEs for the D_{10h} structure were in agreement with the main photoelectron features of NbB$_{10}^-$, while the computed VDEs for the 3D low-lying isomer agreed well with the weak low binding energy features (Fig. 27c and d).

As shown in Fig. 29, chemical bonding analyses using AdNDP for the Ta@B$_{10}^-$ molecular wheel revealed ten 2c-2e B–B bonds, three delocalized π bonds, and five delocalized σ bonds. All the five valence electrons of Ta participate in bonding with the B$_{10}$ ring. The ten delocalized σ electrons also obeyed the $4n + 2$ Huckel rule, again giving rise to double aromaticity for the Ta@B$_{10}^-$ molecular wheel. AdNDP analyses for the Nb@B$_{10}^-$ molecular wheel yielded a similar bonding picture as shown in Fig. 29. Hence, the electronic design principle of eqn (2) needed to be modified to account for the 16 delocalized electrons for double aromaticity, as given in eqn (3).[116]

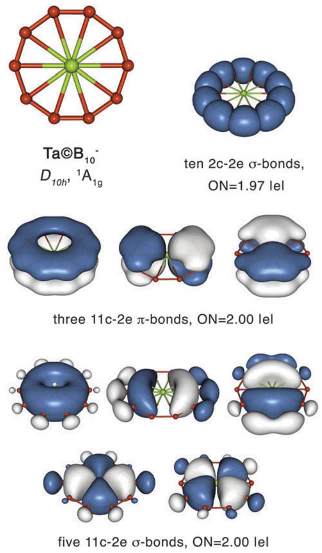

Fig. 29 AdNDP analyses for the D_{10h} Ta@B$_{10}^-$ molecular wheel.[116]

The Ta@B$_{10}^-$ and Nb@B$_{10}^-$ molecular wheels represented the highest coordination number in 2D systems.[131] The metal-centered molecular wheel with larger rings would be challenging, because of the increased M–B distances and the expected weakening of the M–B interactions. This effect was already reflected by the reduced stability of the Nb@B$_{10}^-$ global minimum, relative to the 3D isomer (Fig. 28), as a result of the smaller atomic size of Nb. In fact, for VB$_{10}^-$, it was shown that the 3D structure became the global minimum and the D_{10h} V@B$_{10}^-$ structure became a much higher energy isomer.[120]

5. Concluding remarks and perspectives

In conclusion, we have discussed the applications of the concepts of aromaticity and antiaromaticity in atomic clusters primarily based on research done jointly in the authors' labs over the past fifteen years. Despite of grievances about extending aromaticity beyond benzene or related organic compounds,[132] the concept of aromaticity has found to be highly useful in understanding the structures and bonding of a wide variety of cluster species, resulting in the correct interpretation of similar motifs in synthetic inorganic complexes and solid compounds. The concept was first used to understand the square-planar structure of Al$_4^{2-}$ in a series of bimetallic MAl$_4^-$ clusters that led to the understanding of a similar Ga$_4^{2-}$ motif in a synthetic Ga$_4$ compound and the square-planar Hg$_4$ units in the Na$_3$Hg$_2$ amalgam. Furthermore, aromaticity has been found to play a role in the bonding of transition metal clusters and compounds involving d orbitals. More importantly, aromaticity has been discovered to play a central role in the 2D structures and the properties of size-selected boron clusters. Analogies have been found between the π bonding of most 2D boron clusters and that in polycyclic aromatic hydrocarbons. Stimulated by the observation of doubly σ and π aromaticity in planar boron clusters, an electronic design principle has been proposed for metal-centered aromatic borometallic molecular wheels. A series of such molecular wheels have been produced and characterized experimentally and theoretically, resulting in the discovery of the highest coordination number in 2D systems. Most recently, aromaticity has also been observed in the boron drum in CoB$_{16}^-$.[133] One hundred and fifty years after the introduction of the concept of aromaticity by Kekule to explain the special properties of benzene, the concept is still live and well and is finding more and more applications in chemistry.

Acknowledgements

The experimental work carried out at Brown University was supported by the National Science Foundation (CHE-1263745). The theoretical work done at Utah State University was also supported by the National Science Foundation (CHE-1361413). We are grateful to the contributions of many colleagues both in

Published on 28 January 2016. Downloaded by Brown University on 04/02/2017 04:05:37.

the Wang and Boldyrev groups and outside to the work described and cited in this article.

References

1 A. Kekule, *Bull. Soc. Chim. Fr.*, 1865, **3**, 98.

2 A. Kekule, *Bull. Acad. R. Med. Belg.*, 1865, **119**, 551.

3 A. Kekule, *Ann. Chem.*, 1865, **137**, 129.

4 E. Huckel, *Z. Phys.*, 1931, **70**, 204.

5 E. Huckel, *Z. Phys.*, 1932, **76**, 628.

6 R. Breslow, *Chem. Eng. News*, 1965, **43**, 90, June 28.

7 R. Breslow, *Acc. Chem. Res.*, 1973, **6**, 393.

8 A. I. Boldyrev and L. S. Wang, *Chem. Rev.*, 2005, **105**, 3716–3757.

9 C. A. Tsipis, *Coord. Chem. Rev.*, 2005, **249**, 2740–2762.

10 A. N. Alexandrova, A. I. Boldyrev, H. J. Zhai and L. S. Wang, *Coord. Chem. Rev.*, 2006, **250**, 2811–2866.

11 D. Yu. Zubarev and A. I. Boldyrev, in *Computational Inorganic and Bioinorganic Chemistry*, ed. E. I. Solomon, R. A. Scott and R. Bruce King, John Wiley & Sons, Ltd, Chistester, UK, 2009, pp. 551–562.

12 A. P. Sergeeva, B. B. Averkiev and A. I. Boldyrev, in *Metal-Metal Bonding. Structure and Bonding book series*, ed. G. Parkin, Springer, Berlin/Heidelberg, 2010, **vol. 136**, pp. 275–306.

13 C. A. Tsipis, in *Metal-Metal Bonding. Structure and Bonding book series*, ed. G. Parkin, Springer, Berlin/Heidelberg, 2010, **vol. 136**, pp. 217–274.

14 A. P. Sergeeva and A. I. Boldyrev, in *Aromaticity and Metal Clusters*, ed. P. K. Chattaraj, CRC Press, BocaRaton, 2010, pp. 55–68.

15 T. R. Galeev and A. I. Boldyrev, *Annu. Rep. Prog. Chem., Sect. C: Phys. Chem.*, 2011, **107**, 124–147.

16 F. Feixas, E. Matito, J. Poater and M. Solá, *Wiley Interdiscip. Rev.: Comput. Mol. Sci.*, 2013, **3**, 105–122.

17 I. A. Popov and A. I. Boldyrev, in *The Chemical Bond. Chemical Bonding Across the Periodic Table*, ed. G. Frenking and S. Shaik, Wiley-VCH, Weinheim, 2014, pp. 421–444.

18 J. M. Mercero, A. I. Boldyrev, G. Merino and J. M. Ugalde, *Chem. Soc. Rev.*, 2015, **44**, 6519–6534.

19 A. I. Boldyrev, X. Li and L. S. Wang, *J. Chem. Phys.*, 2000, **112**, 3627–3632.

20 A. I. Boldyrev, X. Li and L. S. Wang, *J. Phys. Chem. A*, 2000, **104**, 5358–5365.

21 A. I. Boldyrev and L. S. Wang, *J. Phys. Chem. A*, 2001, **105**, 10759–10775.

22 X. Li, A. E. Kuznetsov, H. F. Zhang, A. I. Boldyrev and L. S. Wang, *Science*, 2001, **291**, 859–861.

23 D. Y. Zubarev, B. B. Averkiev, H. J. Zhai, L. S. Wang and A. I. Boldyrev, *Phys. Chem. Chem. Phys.*, 2008, **10**, 257–267.

24 X. Li, L. S. Wang, A. I. Boldyrev and J. Simons, *J. Am. Chem. Soc.*, 1999, **121**, 6033–6038.

25 L. S. Wang, A. I. Boldyrev, X. Li and J. Simons, *J. Am. Chem. Soc.*, 2000, **122**, 7681–7687.

26 X. Li, H. F. Zhang, L. S. Wang, G. D. Geske and A. I. Boldyrev, *Angew. Chem., Int. Ed.*, 2000, **39**, 3630–3633.

27 D. Yu. Zubarev and A. I. Boldyrev, *J. Phys. Chem. A*, 2008, **112**, 7984–7985.

28 D. S. Lambrecht, T. Fleig and T. Sommerfeld, *J. Phys. Chem. A*, 2008, **112**, 2855–2862.

29 W. D. Knight, K. Clemenger, W. A. de Heer, W. A. Saunders, M. Y. Chou and M. L. Cohen, *Phys. Rev. Lett.*, 1984, **52**, 2141–2143.

30 F. Catara, Ph. Chomaz and N. V. Giai, *Z. Phys. D: At., Mol. Clusters*, 1995, **33**, 219–227.

31 P. W. Fowler, R. W. A. Havenith and E. Steiner, *Chem. Phys. Lett.*, 2001, **342**, 85–90.

32 P. W. Fowler, R. W. A. Havenith and E. Steiner, *Chem. Phys. Lett.*, 2002, **359**, 530–536.

33 F. Feixas, J. O. C. Jiménez-Halla, E. Matito, J. Poater and M. Solà, *J. Chem. Theory Comput.*, 2010, **6**, 1118–1130.

34 J. Poater, F. Feixas, F. M. Bickelhaupt and M. Solà, *Phys. Chem. Chem. Phys.*, 2011, **13**, 20673–20681.

35 A. E. Kuznetsov, A. I. Boldyrev, X. Li and L. S. Wang, *J. Am. Chem. Soc.*, 2001, **123**, 8825–8831.

36 A. E. Kuznetsov and A. I. Boldyrev, *Inorg. Chem.*, 2002, **41**, 532–537.

37 C. G. Zhan, F. Zheng and D. A. Dixon, *J. Am. Chem. Soc.*, 2002, **124**, 14795–14803.

38 R. W. A. Havenith and J. H. van Lenthe, *Chem. Phys. Lett.*, 2004, **385**, 198–201.

39 X. W. Li, W. T. Pennington and G. H. Robinson, *J. Am. Chem. Soc.*, 1995, **117**, 7578–7579.

40 B. Twamley and P. P. Power, *Angew. Chem., Int. Ed.*, 2000, **39**, 3500–3503.

41 X. Li, H. F. Zhang, L. S. Wang, A. E. Kuznetsov, N. A. Cannon and A. I. Boldyrev, *Angew. Chem., Int. Ed.*, 2001, **40**, 1867–1870.

42 A. Ugrinov, A. Sen, A. C. Reber, M. Qian and S. N. Khanna, *J. Am. Chem. Soc.*, 2008, **130**, 782–783.

43 J. J. Melko, S. V. Ong, U. Gupta, J. U. Reveles, J. D'Emidio, S. N. Khanna and A. W. Castleman Jr., *Chem. Phys. Lett.*, 2010, **500**, 196–201.

44 J. J. Melko, S. V. Ong, U. Gupta, J. U. Reveles, J. D'Emidio, S. N. Khanna and A. W. Castleman Jr., *J. Phys. Chem. C*, 2010, **114**, 20907–20916.

45 A. E. Kuznetsov, K. A. Birch, A. I. Boldyrev, X. Li, H. J. Zhai and L. S. Wang, *Science*, 2003, **300**, 622–625.

46 Z. Chen, C. Cominboeuf, T. Heine, J. Bohmann and P. v. R. Schleyer, *J. Am. Chem. Soc.*, 2003, **125**, 13930.

47 F. Feixas, E. Matito, M. Duran, J. Poater and M. Solà, *Theor. Chem. Acc.*, 2011, **128**, 419–431.

48 S. K. Ritter, *Chem. Eng. News*, 2003, **81**(50), 23.

49 R. W. A. Havenith, P. W. Fowler, E. Steiner, S. Shetty, D. Kanhere and S. Pal, *Phys. Chem. Chem. Phys.*, 2004, **4**, 285.

50 J. C. Santos, J. Andres, A. Aizman and P. Fuentealba, *J. Chem. Theory Comput.*, 2005, **1**, 83–86.

51 S. Chacko, D. G. Kanhere and V. V. Paranjape, *Phys. Rev. A: At., Mol., Opt. Phys.*, 2004, **70**, 023204.

52 S. Shaik, A. Shurki, D. Danovich and P. C. Hiberty, *Chem. Rev.*, 2002, **101**, 1501–1540.

Published on 28 January 2016. Downloaded by Brown University on 04/02/2017 04:05:37.

53 A. Datta and S. K. Pati, *J. Phys. Chem. A*, 2004, **108**, 9527–9530.
54 A. Datta and S. K. Pati, *J. Am. Chem. Soc.*, 2004, **127**, 3496–3500.
55 Y.-C. Lin, J. Juselius, D. Sundholm and J. Gauss, *J. Chem. Phys.*, 2005, **122**, 214308.
56 J. P. Foster and F. Weinhold, *J. Am. Chem. Soc.*, 1980, **102**, 7211–7218.
57 A. E. Reed, R. B. Weinstock and F. Weinhold, *J. Chem. Phys.*, 1985, **83**, 735–746.
58 A. E. Reed, L. A. Curtiss and F. Weinhold, *Chem. Rev.*, 1988, **88**, 899–926.
59 F. Weinhold and C. R. Landis, *Valency and Bonding: A Natural Bond Orbital Donor-Acceptor Perspective*, Cambridge University Press, Cambridge, UK, 2005.
60 D. Y. Zubarev and A. I. Boldyrev, *Phys. Chem. Chem. Phys.*, 2008, **10**, 5207–5217.
61 B. D. Dunnington and J. R. Schmidt, *J. Chem. Theory Comput.*, 2012, **8**, 1902–1911.
62 T. R. Galeev, B. D. Dunnington, J. R. Schmidt and A. I. Boldyrev, *Phys. Chem. Chem. Phys.*, 2013, **15**, 5022–5029.
63 J. W. Nielsen and N. C. Baenziger, *Acta Crystallogr.*, 1954, **7**, 277–282.
64 J. D. Corbett, *Inorg. Nucl. Chem. Lett.*, 1969, **5**, 81–84.
65 A. E. Kuznetsov, J. D. Corbett, L. S. Wang and A. I. Boldyrev, *Angew. Chem., Int. Ed.*, 2001, **40**, 3369–3372.
66 I. Todorov and S. C. Sevov, *Inorg. Chem.*, 2004, **43**, 6490–6494.
67 A. N. Alexandrova and A. I. Boldyrev, *J. Phys. Chem. A*, 2003, **107**, 554–560.
68 J. Ivanic, C. J. Marsden and D. M. Hassett, *J. Chem. Soc., Chem. Commun.*, 1993, 822–825.
69 E. Jimenez-Izal and A. N. Alexandrova, *Phys. Chem. Chem. Phys.*, 2015, DOI: 10.1039/c5cp04330a.
70 X. Huang, H. J. Zhai, B. Kiran and L. S. Wang, *Angew. Chem., Int. Ed.*, 2005, **44**, 7251–7254.
71 H. J. Zhai, B. B. Averkiev, D. Y. Zubarev, L. S. Wang and A. I. Boldyrev, *Angew. Chem., Int. Ed.*, 2007, **46**, 4277–4280.
72 H. J. Zhai, B. Wang, X. Huang and L. S. Wang, *J. Phys. Chem.*, 2009, **113**, 9804–9813.
73 H. J. Zhai, B. Wang, X. Huang and L. S. Wang, *J. Phys. Chem. A*, 2009, **113**, 3866–3875.
74 W. J. Chen, H. J. Zhai, Y. F. Zhang, X. Huang and L. S. Wang, *J. Phys. Chem. A*, 2010, **114**, 5958–5966.
75 A. S. Ivanov, X. Zhang, H. Wang, A. I. Boldyrev, G. F. Gantefoer, K. H. Bowen Jr. and I. Černušàk, *J. Phys. Chem. A*, 2015, **119**, 11293–11303.
76 B. B. Averkiev and A. I. Boldyrev, *J. Phys. Chem. A*, 2007, **111**, 12864–12866.
77 T. Murahashi, R. Inoue, K. Usui and S. Ogoshi, *J. Am. Chem. Soc.*, 2009, **131**, 9888–9889.
78 A. P. Sergeeva and A. I. Boldyrev, *Phys. Chem. Chem. Phys.*, 2010, **12**, 12050–12054.
79 S. Blanchard, L. Fensterbank, G. Gontard, E. Lacote, G. Maestri and M. Malacria, *Angew. Chem., Int. Ed.*, 2014, **53**, 1987–1991.
80 T. Kuwabara, J. D. Guo, S. Nagase and M. Saito, *Angew. Chem., Int. Ed.*, 2014, **53**, 434–438.
81 T. J. Robilotto, J. Bacsa, T. B. Gray and J. P. Sadighi, *Angew. Chem., Int. Ed.*, 2012, **51**, 12077–12080.
82 K. Freitag, C. Gemel, P. Jerabek, M. I. Oppel, R. W. Seidel, G. Frenking, H. Banh, K. Dilchert and R. A. Fischer, *Angew. Chem., Int. Ed.*, 2015, **54**, 4370–4374.
83 A. E. Kuznetsov, A. I. Boldyrev, H. J. Zhai, X. Li and L. S. Wang, *J. Am. Chem. Soc.*, 2002, **124**, 11791–11801.
84 A. Hirsch, Z. Chen and H. Jiao, *Angew. Chem., Int. Ed.*, 2000, **39**, 3915–3917.
85 H.-C. Hu, H.-S. Hu, B. Zhao, P. Cui, P. Cheng and J. Li, *Angew. Chem., Int. Ed.*, 2015, **54**, 11681–11685.
86 P. Cui, H.-S. Hu, B. Zhao, J. T. Miller, P. Cheng and J. Li, *Nat. Commun.*, 2015, **6**, 6331.
87 X. Yu, A. R. Oganov, I. A. Popov and A. I. Boldyrev, *J. Comput. Chem.*, 2016, **37**, 103–109.
88 M. Walker, J. Akola, O. Lopez-Acevedo, P. D. Jadzinsky, G. Calero, C. J. Ackerson, R. L. Whetten, H. Gronbeck and H. Hakkinen, *Proc. Natl. Acad. Sci. U. S. A.*, 2008, **105**, 9157–9162.
89 D. Y. Zubarev and A. I. Boldyrev, *J. Comput. Chem.*, 2007, **28**, 251–268.
90 A. P. Sergeeva, I. A. Popov, Z. A. Piazza, W. L. Li, C. Romanescu, L. S. Wang and A. I. Boldyrev, *Acc. Chem. Res.*, 2014, **47**, 1349–1358.
91 L. S. Wang, *Int. Rev. Phys. Chem.*, 2016, **35**, in press.
92 H. J. Zhai, A. N. Alexandrova, K. A. Birch, A. I. Boldyrev and L. S. Wang, *Angew. Chem., Int. Ed.*, 2003, **42**, 6004–6008.
93 H. J. Zhai, B. Kiran, J. Li and L. S. Wang, *Nat. Mater.*, 2003, **2**, 827–833.
94 A. Ricca and C. W. Bauschlicher Jr., *Chem. Phys. Lett.*, 1996, **208**, 233–242.
95 J. E. Fowler and J. M. Ugalde, *J. Phys. Chem. A*, 2000, **104**, 397–403.
96 A. P. Sergeeva, D. Yu. Zubarev, H. J. Zhai, A. I. Boldyrev and L. S. Wang, *J. Am. Chem. Soc.*, 2008, **130**, 7244–7246.
97 C. Romanescu, D. J. Harding, A. Fielicke and L. S. Wang, *J. Chem. Phys.*, 2012, **137**, 014317.
98 E. Oger, N. R. M. Crawford, R. Kelting, P. Weis, M. M. Kappes and R. Ahlrichs, *Angew. Chem., Int. Ed.*, 2007, **46**, 8503–8506.
99 A. P. Sergeeva, B. B. Averkiev, H. J. Zhai, A. I. Boldyrev and L. S. Wang, *J. Chem. Phys.*, 2011, **134**, 224304.
100 W. Huang, A. P. Sergeeva, H. J. Zhai, B. B. Averkiev, L. S. Wang and A. I. Boldyrev, *Nat. Commun.*, 2010, **2**, 202–206.
101 J. O. C. Jimenez-Halla, R. Islas, T. Heine and G. Merino, *Angew. Chem., Int. Ed.*, 2010, **49**, 5668–5671.
102 D. Moreno, S. Pan, L. L. Zeonjuk, R. Islas, E. Osorio, G. Martinez-Guajardo, P. K. Chattaraj, T. Heine and G. Merino, *Chem. Commun.*, 2014, **50**, 8140–8143.
103 Z. A. Piazza, W. L. Li, C. Romanescu, A. P. Sergeeva, L. S. Wang and A. I. Boldyrev, *J. Chem. Phys.*, 2012, **136**, 104310.
104 A. P. Sergeeva, Z. A. Piazza, C. Romanescu, W. L. Li, A. I. Boldyrev and L. S. Wang, *J. Am. Chem. Soc.*, 2012, **134**, 18065–18073.

Published on 28 January 2016. Downloaded by Brown University on 04/02/2017 04:05:37.

105 Z. A. Piazza, H. S. Hu, W. L. Li, Y. F. Zhao, J. Li and L. S. Wang, *Nat. Commun.*, 2014, **5**, 3113.

106 Q. Chen, G. F. Wei, W. J. Tian, H. Bai, Z. P. Liu, H. J. Zhai and S. D. Li, *Phys. Chem. Chem. Phys.*, 2015, **16**, 18282–18287.

107 H. Tang and S. Ismail-Beigi, *Phys. Rev. Lett.*, 2007, **99**, 115501.

108 X. Yang, Y. Ding and J. Ni, *Phys. Rev. B: Condens. Matter Mater. Phys.*, 2008, **77**, 041402.

109 W. L. Li, Q. Chen, W. J. Tian, H. Bai, Y. F. Zhao, H. S. Hu, J. Li, H. J. Zhai, S. D. Li and L. S. Wang, *J. Am. Chem. Soc.*, 2014, **136**, 12257–12260.

110 E. S. Penev, S. Bhowmick, A. Sadrzadeh and B. I. Yakobson, *Nano Lett.*, 2012, **12**, 2441–2445.

111 X. Wu, J. Dai, Y. Zhao, A. Zhuo, J. Yang and X. C. Zeng, *ACS Nano*, 2012, **6**, 7443–7453.

112 H. J. Zhai, Y. F. Zhao, W. L. Li, Q. Chen, H. Bai, H. S. Hu, Z. A. Piazza, W. J. Tian, H. G. Lu, Y. B. Wu, Y. W. Mu, G. F. Wei, Z. P. Liu, J. Li, S. D. Li and L. S. Wang, *Nat. Commun.*, 2014, **6**, 727–731.

113 D. M. Hudgins, C. W. Bauschlicher Jr and L. J. Allamandola, *Spectrochim. Acta, Part A*, 2001, **57**, 907–930.

114 C. Romanescu, T. R. Galeev, W. L. Li, A. I. Boldyrev and L. S. Wang, *Angew. Chem., Int. Ed.*, 2011, **50**, 9334–9337.

115 W. L. Li, C. Romanescu, T. R. Galeev, Z. A. Piazza, A. I. Boldyrev and L. S. Wang, *J. Am. Chem. Soc.*, 2012, **134**, 165–168.

116 T. R. Galeev, C. Romanescu, W. L. Li, L. S. Wang and A. I. Boldyrev, *Angew. Chem., Int. Ed.*, 2012, **51**, 2101–2105.

117 C. Romanescu, T. R. Galeev, A. P. Sergeeva, W. L. Li, L. S. Wang and A. I. Boldyrev, *J. Organomet. Chem.*, 2012, **721–722**, 148–154.

118 C. Romanescu, T. R. Galeev, W. L. Li, A. I. Boldyrev and L. S. Wang, *J. Chem. Phys.*, 2013, **138**, 134315.

119 W. L. Li, A. S. Ivanov, J. Federic, C. Romanescu, I. Cernusak, A. I. Boldyrev and L. S. Wang, *J. Chem. Phys.*, 2013, **139**, 104312.

120 W. L. Li, C. Romanescu, Z. A. Piazza and L. S. Wang, *Phys. Chem. Chem. Phys.*, 2012, **14**, 13663–13669.

121 I. A. Popov, W. L. Li, Z. A. Piazza, A. I. Boldyrev and L. S. Wang, *J. Phys. Chem. A*, 2014, **118**, 8098–8105.

122 C. Romanescu, A. P. Sergeeva, W. L. Li, A. I. Boldyrev and L. S. Wang, *J. Am. Chem. Soc.*, 2011, **133**, 8646–8653.

123 T. R. Galeev, C. Romanescu, W. L. Li, L. S. Wang and A. I. Boldyrev, *J. Chem. Phys.*, 2011, **135**, 104301.

124 W. L. Li, C. Romanescu, T. R. Galeev, L. S. Wang and A. I. Boldyrev, *J. Phys. Chem. A*, 2011, **115**, 10391–10397.

125 B. B. Averkiev and A. I. Boldyrev, *Russ. J. Gen. Chem.*, 2008, **78**, 769–773.

126 R. Islas, T. Heine, K. Ito, P. v. R. Schleyer and G. Merino, *J. Am. Chem. Soc.*, 2007, **129**, 14767–14774.

127 C. Romanescu, T. R. Galeev, W. L. Li, A. I. Boldyrev and L. S. Wang, *Acc. Chem. Res.*, 2013, **46**, 350–358.

128 H. J. Zhai, L. S. Wang, D. Y. Zubarev and A. I. Boldyrev, *J. Phys. Chem. A*, 2006, **110**, 1689–1693.

129 L. S. Wang, *Phys. Chem. Chem. Phys.*, 2010, **12**, 8694–8705.

130 H. J. Zhai, C. Q. Miao, S. D. Li and L. S. Wang, *J. Phys. Chem. A*, 2010, **114**, 12155–12161.

131 T. Heine and G. Merino, *Angew. Chem., Int. Ed.*, 2012, **51**, 4275–4276.

132 S. K. Ritter, *Chem. Eng. News*, 2015, **93**(8), 37–38.

133 A. Popov, T. Jian, G. V. Lopez, A. I. Boldyrev and L. S. Wang, *Nat. Commun.*, 2015, **6**, 8654.